AMMRC TR 75-19

AD

THE PARTITIONING OF IMPURITY ELEMENTS IN IRON-CARBON ALLOYS

WEILY F. CHIAO, GORDON A. BRUGGEMAN, and ERIC B. KULA
METALS RESEARCH DIVISION

September 1975

ARMY MATERIALS AND MECHANICS RESEARCH CENTER
Watertown, Massachusetts 02172

The findings in this report are not to be construed as an official Department of the Army position, unless so designated by other authorized documents.

Mention of any trade names or manufacturers in this report shall not be construed as advertising nor as an official indorsement or approval of such products or companies by the United States Government.

DISPOSITION INSTRUCTIONS

Destroy this report when it is no longer needed.
Do not return it to the originator.

UNCLASSIFIED

SECURITY CLASSIFICATION OF THIS PAGE (When Data Entered)

REPORT DOCUMENTATION PAGE	READ INSTRUCTIONS BEFORE COMPLETING FORM
1. REPORT NUMBER: AMMRC-TR-75-19	2. GOVT ACCESSION NO. / 3. RECIPIENT'S CATALOG NUMBER
4. TITLE (and Subtitle): THE PARTITIONING OF IMPURITY ELEMENTS IN IRON-CARBON ALLOYS	5. TYPE OF REPORT & PERIOD COVERED: Final Report
	6. PERFORMING ORG. REPORT NUMBER
7. AUTHOR(s): Weily F. Chiao, Gordon A. Bruggeman and Eric B. Kula	8. CONTRACT OR GRANT NUMBER(s)
9. PERFORMING ORGANIZATION NAME AND ADDRESS: Army Materials and Mechanics Research Center, Watertown, Massachusetts 02172, AMXMR-M	10. PROGRAM ELEMENT, PROJECT, TASK AREA & WORK UNIT NUMBERS: D/A Project: 1T162105AH84; AMCMS Code: 62105.11.H8400; Agency Accession: DA 0A4700
11. CONTROLLING OFFICE NAME AND ADDRESS: U. S. Army Materiel Command, Alexandria, Virginia 22333	12. REPORT DATE: Sep 75 / 13. NUMBER OF PAGES: 42 (46p.)
14. MONITORING AGENCY NAME & ADDRESS (if different from Controlling Office): DA-1-T-162105-HH-84	15. SECURITY CLASS. (of this report): Unclassified
	15a. DECLASSIFICATION/DOWNGRADING SCHEDULE

16. DISTRIBUTION STATEMENT (of this Report)

Approved for public release; distribution unlimited.

17. DISTRIBUTION STATEMENT (of the abstract entered in Block 20, if different from Report)

18. SUPPLEMENTARY NOTES

19. KEY WORDS (Continue on reverse side if necessary and identify by block number)

Equilibrium	Ferrite	Silicon
Chemical composition	Impurities	Antimony
Carbides	Tin	Arsenic
Steels	Phosphorus	

20. ABSTRACT (Continue on reverse side if necessary and identify by block number)

(SEE REVERSE SIDE)

DD FORM 1 JAN 73 1473 EDITION OF 1 NOV 65 IS OBSOLETE

UNCLASSIFIED

403105

SECURITY CLASSIFICATION OF THIS PAGE (When Data Entered)

Block No. 20

ABSTRACT

The partitioning at 600 C of the elements tin, phosphorus, silicon, antimony, and arsenic between the ferrite and carbide phases was investigated in Fe-C-X alloys, where X is one of the above elements. These elements are all known to increase the susceptibility for temper brittleness in steels and are suspected of playing a similar role in the phenomenon of tempered martensite embrittlement or 500 F embrittlement. The procedures of metallographic examination, electron microprobe analysis, ferrite lattice parameter measurement, and chemical analysis and crystal structure determination of extracted carbides were employed in the study. It was determined that of the above elements only tin and phosphorus appear to partition to the carbide phase, tin apparently forming a ternary carbide. The remaining elements silicon, antimony, and arsenic partition to ferrite, thus providing a condition conducive to the accumulation of these impurities on the ferrite side of ferrite/carbide interfaces during tempering. By virtue of its more potent solid solution strengthening effect in ferrite, one might, therefore, anticipate a greater embrittling tendency from the impurity element antimony, a prediction borne out by experiment. Solubility limits, distribution coefficients, and other phase relations were determined during the course of this study. (Authors)

CONTENTS

INTRODUCTION

The phenomenon of temper brittleness has been found to be closely associated with the presence of certain impurity elements in alloy steels which have been tempered in or slowly cooled through the 575 to 325 C temperature range.[1-9] For recent detailed discussions of temper brittleness, the reader is referred to reviews by McMahon[10] and by Narayan and Murphy.[11] The impurities antimony, arsenic, tin, phosphorus, and silicon appear to render the steel particularly susceptible to temper brittleness, even though these elements may be present only in trace amounts. The opinion is generally held that temper brittleness involves the reversible segregation of these impurity elements to grain boundaries during tempering, although the precise details of the embrittlement mechanism remain obscure.

It has been suggested that a related form of segregation of these same impurities is responsible for the phenomenon of tempered martensite embrittlement or 500 F embrittlement.[5,12-16] Indeed it has been reported that 500 F embrittlement was not encountered in high-purity steels from which the elements antimony, arsenic, tin, and phosphorus were absent.[5,12,13] The proposed mechanism to account for this effect suggests that substitutional impurities having low mobilities are rejected by the carbides formed during tempering[15] or are swept ahead of the advancing ferrite/carbide interface.[16] The impurities thus rejected accumulate at the ferrite/carbide interface and cause embrittlement in the same manner that adsorbed impurities would. The viability of this mechanism depends, of course, upon the partitioning of impurities between ferrite and the carbides formed during tempering (Fe_3C in this range of tempering temperatures). It has been the objective of this investigation, therefore, to determine the equilibrium partitioning of certain known or suspected embrittling impurities between the ferrite and carbide phases, in order to provide the background data necessary for the evaluation of these embrittlement mechanisms. In so doing, various phase relations have been determined in the Fe-C-X ternary alloy systems, where X is one of the impurity elements antimony, arsenic, tin, phosphorus, and silicon.

1. STEVEN, W., and BALAJIVA, K. *The Influence of Minor Elements on the Isothermal Embrittlement of Steels.* J. Iron Steel Inst., v. 193, 1959, p. 141-147.
2. JOLIVET, H., and VIDAL, G. *Valeur de l'essai de resilience pour l'etude de la fragilite de revenu.* Rev. Met., v. 41, 1944, p. 378-388.
3. AUSTIN, G. W., ENTWISLE, A. R., and SMITH, G. C. *Effect of Arsenic and Antimony on Temper-Brittleness.* J. Iron Steel Inst., v. 173, 1953, p. 376-386.
4. PREECE, A., and CARTER, R. D. *Temper Brittleness in High-Purity Iron-Base Alloys.* J. Iron Steel Inst., v. 173, 1953, p. 387-398.
5. CAPUS, J. M., and MAYER, G. *The Influence of Trace Elements on Embrittlement Phenomena in Low-Alloy Steels.* Metallurgia, v. 62, 1960, p. 133-138.
6. CAPUS, J. M. *Austenite Grain Size and Temper Brittleness.* J. Iron Steel Inst., v. 200, 1962, p. 922-927.
7. BARON, H. G., and TURNER, S. *Effects of Residual Elements on Brittleness in Hardened and Tempered Forgings of Nickel-Chromium-Molybdenum Steel.* J. Iron Steel Inst., v. 203, 1965, p. 1229-1236.
8. RESTAINO, P. A., and McMAHON, C. J., Jr. *The Role of Antimony in Temper Brittleness.* Trans. ASM, v. 60, 1967, p. 699-706.
9. LOW, J. R., Jr., STEIN, D. F., TURKALO, A. M., and LaFORCE, R. P. *Alloy and Impurity Effects on Temper Brittleness of Steel.* Trans. TMS-AIME, v. 242, 1968, p. 14-24.
10. McMAHON, C. J., Jr. *Temper Brittleness--An Interpretive Review* in Temper Embrittlement in Steel, ASTM-STP 407, ASTM, Philadelphia, 1968, p. 127-167.
11. NARAYAN, R., and MURPHY, M. C. *A Review of Temper Embrittlement as it Affects Major Steam Turbine and Generator Rotor Forgings.* J. Iron Steel Inst., v. 211, 1973, p. 493-501.
12. CAPUS, J. M. *L'influence d'oligo-elements sur la resilience des aciers foiblement allies, trempes et revenus.* Rev. Met., v. 56, 1959, p. 181-187.
13. CAPUS, J. M. *Carbide Precipitation, Impurity Elements, and the Embrittlement of High-Strength Martensitic Alloy Steels.* J. Iron Steel Inst., v. 201, 1963, p. 53-54.
14. BRUGGEMAN, G. A., and KULA, E. B. *Segregation at Interphase Interfaces* in Surfaces and Interfaces, v. II, Syracuse University Press, Syracuse, 1968, p. 455-480.
15. KULA, E. B., and ANCTIL, A. A. *Tempered Martensite Embrittlement and Fracture Toughness in 4340 Steel.* J. Matls., v. 4, 1969, p. 817-841.
16. RELLICK, J. R., and McMAHON, C. J., Jr. *Intergranular Embrittlement of Iron Carbon Alloys by Impurities.* Met. Trans., v. 5, 1974, p. 2439-2450.

This work has been limited, for the most part, to an investigation of phase relations in the iron-rich corner of the Fe-C-X ternary phase diagram at a temperature of 600 C, although a limited amount of data were obtained at other temperatures as well. The 600 C temperature was selected primarily because it was felt that thermodynamic equilibrium between the various phases, and also structures of sufficient metallographic coarseness, could not conveniently be obtained below this temperature. Furthermore, because of the close proximity of the temper brittleness temperature range and because no equilibrium phase changes occur at lower temperatures in any of the alloy systems under investigation, the data are expected to be of significance in the mechanisms of both temper brittleness and tempered martensite embrittlement.

EXPERIMENTAL ALLOYS

Both binary Fe-X and ternary Fe-C-X alloys were made up using Ferrovac E of 99.98% Fe containing 0.002% O and 0.002% C.* The carbon addition was high purity graphite and the alloying additions were of the highest purity readily available. Alloys were nonconsumably arc melted under argon three times and cast into 2-inch cubes. The ingots of lower alloy content were then heated to 800 C under argon and hot pressed to 1/2-inch-thick plate, but the ingots of higher alloy contents were too brittle to be forged and so were heat treated directly in the as-cast condition. The chemical analyses of the alloys studied are presented in tables in the Results and Discussion section.

Heat treatments were devised with the object of obtaining coarse equilibrium microstructures at the desired temperature of 600 C. For this purpose various exploratory heat treatment procedures were carried out on the alloy series containing antimony. Homogenization was performed at temperatures in the range 900 to 1200 C, followed by slow cooling to 600 C and holding at that temperature for various time intervals from two weeks to one month. Based on these preliminary studies, the eventual heat treatment settled upon involved homogenizing at 800 to 900 C (depending upon the alloy), furnace cooling to 600 C, and holding at 600 C for a period of two weeks, followed by water quenching to room temperature. All heat treatments were carried out on specimens encapsulated in quartz ampules which had been purged with argon and then evacuated to 10^{-6} torr. Several of the alloys were found to remain quite inhomogeneous in spite of all efforts to obtain homogeneity.

EXPERIMENTAL PROCEDURES

Specimens were examined metallographically and the chemical compositions of the phases encountered in the various alloy systems determined by electron probe analysis where possible. In addition, the solubility of element X in ferrite and information on the partitioning of element X between the ferrite and carbide phases were determined from measurements of the ferrite lattice parameter. Finally, carbides were extracted from several of the alloys, analyzed chemically, and their crystal structures examined by X-ray diffraction. Details of these procedures follow.

*Concentrations throughout this report will be given in weight percent.

Electron Probe Analysis

Electron probe microanalysis was used to determine the composition of the phases in a number of the alloys. An AMR electron beam microanalyzer with a focus <1 μ in diameter was employed. As in an X-ray tube, the element to be investigated in the specimen acts as a primary source of X rays. The analysis of the characteristic X-ray lines was done by means of two curved mica crystal focusing spectrometers set up to record the various X-ray lines of the alloying elements. The resulting X-ray intensity of the investigated alloying element from each location in the microstructure was then counted and recorded. The observed X-ray intensities of the investigated element were converted to concentrations utilizing calibration standards available in the laboratory.

Carbide Extraction

Based upon previous studies involving the electrolytic extraction of carbides,[17-20] two procedures were investigated. The first utilized a two-compartment electrolytic cell in which a 10% HCl solution was used as the anolyte and a 10% $CuSO_4 \cdot 5H_2O$ solution as the catholyte. The second technique employed a single cell containing a 10% HCl solution in ethyl alcohol in which the alloy specimen, about 1/2-inch in diameter and 2 inches long, served as the anode and a platinum net as the cathode. The latter procedure proved simpler and more convenient and gave satisfactory results, and so the bulk of the carbide extracts were collected using this technique. It took about 48 to 60 hours at a very low current density of about 0.01 amp/cm^2 to collect enough carbide for chemical and X-ray analyses. The carbides that accumulated on the specimen surface were scraped lightly from the specimen, washed several times in water, alcohol, and finally ether, and then collected for analysis. On several occasions the collected carbides were pyrophoric and began to burn as soon as they were dried. This tendency to rapidly convert to oxide may have been responsible for some spurious X-ray diffraction peaks to be reported on later, in that the final specimen may have actually been a mixture of the carbide and unknown oxides. However, this aspect should not have seriously affected the chemical analyses insofar as the concentration of element X is concerned.

X-Ray Diffraction

All the ferrite lattice parameter data were obtained from solid specimens. The lattice parameters were measured at 24 ±1 C using an X-ray diffractometer with cobalt radiation. Diffraction peaks were obtained at 2θ angles from 50° to 160°. In most specimens the peak profile was symmetrical so that the value of 2θ was determined by simple bisection of the peak. An average of twenty peaks were measured per specimen. A least-squares extrapolation of the lattice parameter

17. KUO, K. *Isolation of Carbide Residues and Their Analysis*, appendix in: Isothermal Transformation of Austenite and Partitioning of Alloying Elements in Low Alloy Steels, A. Hultgren and Collaborators, ed., Kungl. Svenska Vetenskapsakademiens Handlingar, Fourth Series, 4, no. 3, Almqvist and Wiksells Boktryckeri AB, Stockholm, 1953.
18. TREJE, R., and BENEDICKS, C. *A Method for the Electrolytic Extraction of Slag From Iron and Carbon Steel.* J. Iron Steel Inst., v. 128, 1933, p. 205-230.
19. BLICKWEDE, D. J., and COHEN, M. *The Isolation of Carbides from High Speed Steel.* Trans. AIME, v. 185, 1949, p. 578-584.
20. KLINGLER, L. J., BARNETT, W. J., FROHMBERG, R. P., and TROIANO, A. R. *The Embrittlement of Alloy Steel at High Strength Levels.* Trans. ASM, v. 46, 1954, p. 1557-1589.

data with cotθ was made to the value at θ = 90°. With this procedure lattice parameters with a precision of ±0.0001 Å could normally be expected.

Carbide lattice parameters were obtained from the extracted carbides using an X-ray diffractometer with chromium radiation. The amount of powder that could be obtained in several instances was small, giving rise to rather broad diffraction peaks. The observed peaks were indexed assuming the structure to be orthorhombic in which the alloying element X has been substituted for iron atoms in the cementite structure to produce a $(Fe,X)_3C$ type carbide. The carbide lattice parameters were calculated by a method of weighted least squares[21] which assumed the measured cell parameters to be affected by absorption and beam divergence in a manner suggested by Nelson and Riley.[22] The resulting unit cell dimensions cannot be considered very precise, but they are of sufficient accuracy to establish qualitative trends in the data.

PHASE RELATIONS DERIVED FROM FERRITE LATTICE PARAMETER DATA

In most instances the ferrite lattice parameters of a series of binary Fe-X alloys will vary linearly with the concentration of X as shown schematically in Figure 1. The change in lattice parameter reflects the changing proportions of atoms of different atomic radii in a substitutional solid solution. The lattice parameter no longer changes with composition as soon as the alloy composition falls within the two-phase region of the phase diagram, due to the fact that the composition of the ferrite has become fixed at the value characteristic of the phase boundary. Thus the solid solubility of element X in ferrite is determined by the point at which the lattice parameter becomes constant in binary Fe-X alloys (point b in Figure 1), a well-known result.

Similarly for a series of Fe-C-X alloys with a fixed carbon content lying in the "ferrite + carbide" two-phase region of the ternary phase diagram, the ferrite lattice parameter will also vary more or less linearly with the concentration of X. If one makes the assumption that carbon dissolved in ferrite affects the ferrite lattice parameter insignificantly compared with the effect of the substitutional element X (an assumption borne out by subsequent lattice parameter measurements), then the ferrite composition is easily obtained. An Fe-C-X alloy with overall concentration x_o has the ferrite lattice parameter indicated in Figure 1, which in turn corresponds to the ferrite composition x_α that in this case is richer in X than the alloy as a whole.

The plot of ferrite lattice parameter versus percentage of X in Fe-C-X alloys with fixed carbon contents will remain linear until the boundary separating the two-phase region from the "ferrite + carbide + intermetallic" three-phase region is reached. The ferrite in all alloys lying in the three-phase region is of fixed composition and hence of constant lattice parameter. Thus the composition at which the ferrite lattice parameter becomes constant in Fe-C-X alloys is the *alloy* composition at the boundary between the two-phase and the three-phase

21. COX, A. A., and STEWARD, E. G. *An I.C.T. Fortran Program for Least-Squares Refinement of Crystal-Structure Cell Dimensions.* Acta Cryst., v. 23, 1967, p. 1113-1114.
22. NELSON, J. B., and RILEY, D. P. *An Experimental Investigation of Extrapolation Methods in the Derivation of Accurate Unit-Cell Dimensions of Crystals.* Proc. Roy. Soc., London, v. 57, 1945, p. 160-177.

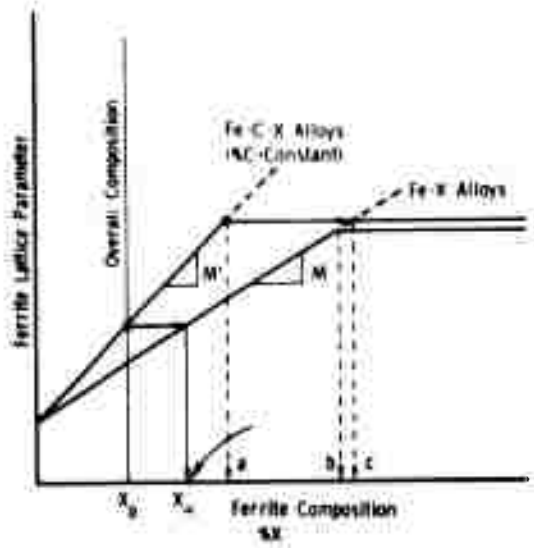

Figure 1. A schematic plot of the ferrite lattice parameter versus concentration of substitutional alloying element X in Fe-X binary alloys and Fe-C-X ternary alloys. Point b defines the limit of solid solubility of X in ferrite in Fe-X alloys. Point a defines the concentration of X in Fe-C-X alloys of that particular carbon content at which the alloy microstructure begins to contain three phases, and point c defines the corresponding ferrite concentration.

regions (point a in Figure 1), and the corresponding ferrite composition (point c in Figure 1) represents the solubility limit of X in ferrite saturated with carbon.

Within the ferrite single-phase field the ferrite lattice parameter can be expressed as

$$a(x_\alpha) = a(o) + Mx_\alpha \qquad (1)$$

where a(o) is the lattice parameter of pure alpha iron, x_α is the percent of element X in the ferrite (which also is the percent of element X in the binary alloy), and M is the slope of the line in Figure 1. If one assumes as before that the ferrite lattice parameter is insignificantly affected by carbon, then Equation (1) also describes the ferrite lattice parameter in ternary Fe-C-X alloys as well, provided x is the percent of element X in the ferrite alone. Assuming further that the distribution ratio of element X in the carbide to X in the ferrite, x_C/x_α, is constant at a constant temperature within the two-phase region of the ternary phase diagram, then the concentration x_α of X in ferrite is proportional to the concentration x_o of X in the alloy as a whole, where the proportionality constant is a function of the distribution ratio and of the carbon content. Therefore, the ferrite lattice parameter in a series of ternary Fe-C-X alloys with a fixed carbon content can also be described by an equation of the same form as Equation (1), but in which x is the percent of element X in the alloy and M takes on a new value characteristic of this particular ternary series.

Referring to the schematic isothermal section through the Fe-C-X phase diagram in Figure 2, the concentration of X in the ferrite is given by

$$x_\alpha = x_o - m(c_o - c_\alpha) \qquad (2)$$

where c_o is the percent carbon in the alloy, c_α is the carbon content of the ferrite, m is the slope of the tie line in the "ferrite + carbide" two-phase field, and the carbon content of the ferrite and of the carbide are both assumed to be negligibly affected by X. Combining (1) and (2), the ferrite lattice parameter in a ternary alloy becomes:

$$a(x) = a(o) + M(x_o - mc_o')$$
$$= a(o) + [M(1 - mc_o'/x_o)]x_o \qquad (3)$$

where $c_o' = c_o - c_\alpha$. Thus a plot of the ferrite lattice parameter in ternary Fe-C-X alloys of constant carbon content versus the total concentration x_o is also linear, with an effective slope M' given by the term in the square brackets, i.e.,

$$M' = M(1 - mc_o'/x_o) . \qquad (4)$$

If the slope m of the tie line is negative (as illustrated in Figure 2), then $|M'|$ is greater than $|M|$ as shown in Figure 1. This will correspond to a ferrite composition x_α that is richer in X than the overall alloy composition, which of course must be balanced by a depletion of element X from the carbide and therefore $x_C < x_\alpha$. Should $|M'|$ be less than $|M|$, the reverse is true, namely $x_C > x_\alpha$. The ratio k of the concentration in the carbide to the concentration in the ferrite, x_C/x_α, may be expressed quantitatively in terms of the measured changes in lattice parameter as follows:

From Figure 2

$$m = \frac{x_C - x_\alpha}{6.65} = \frac{x_\alpha(k - 1)}{6.65} . \qquad (5)$$

Combining (2) and (5),

$$m = \frac{(x_o - mc_o')(k - 1)}{6.65} \qquad (6)$$

which leads ultimately to

$$m = \frac{x_o(k - 1)}{c_o'(k - 1) + 6.65} . \qquad (7)$$

Inserting this result into (4) yields

$$M' = M\left[1 - \frac{c_o'(k - 1)}{c_o'(k - 1) + 6.65}\right]$$
$$= M\left[\frac{6.65}{c_o'(k - 1) + 6.65}\right] . \qquad (8)$$

Rearranging terms gives the desired result

$$k = 1 + \frac{6.65(M - M')}{M'c_o'} . \qquad (9)$$

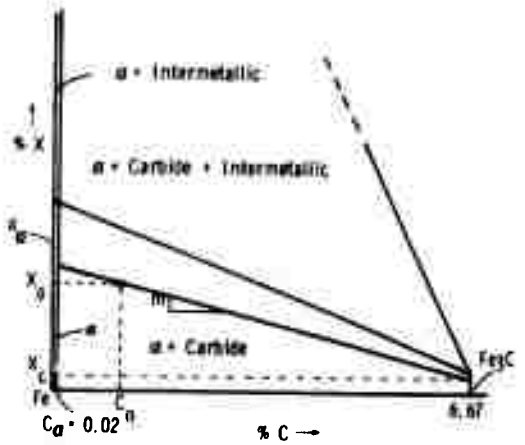

Figure 2. Schematic Fe-C-X ternary phase diagram.

Thus if M' > M (as in Figure 1), k < 1 and the ferrite is richer in X than the carbide. If M' < M, then k > 1 and the carbide is richer in X than the ferrite. M' = M implies that X shows no preference for partitioning to either the ferrite phase or the carbide phase. Therefore, within the framework of the assumptions stated previously, the experimental measurement of ferrite lattice parameters in single-phase binary Fe-X alloys and in two-phase Fe-C-X alloys can, in principle, enable the determination of the distribution coefficient k, provided M and M' can be measured with sufficient accuracy. The stringency of this latter requirement becomes apparent when one considers that in ternary alloys containing about 0.7% carbon, a distribution ratio k = 2 results in only a 10% difference between M and M'.

In this study, M and M' were normally determined from a least-squares regression analysis of the lattice parameter data. In some instances, however, it was not possible to make up a complete alloy series with a constant carbon content. When this occurred, the lattice parameter measured in an individual Fe-C-X alloy could be used independently to determine k by assuming

$$M' = \frac{a(x_o) - a(o)}{x_o}$$

which results in

$$k = 1 + \frac{6.65\,[Mx_o - a(x_o) + a(o)]}{[a(x_o) - a(o)]c_o'} \qquad (10)$$

From a statistical standpoint, this is a less desirable procedure to follow than that leading to Equation (9).

RESULTS AND DISCUSSION

Fe-Sn and Fe-Sn-C Alloys

The published Fe-Sn binary phase diagram[23] is shown in Figure 3. The alloy series containing tin may be divided into three groups (see Table 1): (1) a binary Fe-Sn series (%C∿0.02); (2) a low-carbon series (%C∿0.26); and (3) a medium-carbon series (%C∿0.45). The microstructures of several alloys homogenized at 900 C and annealed at 600 C for two weeks are shown in Figures 4 to 6. The binary Fe-Sn series is totally ferritic until the tin content exceeds that of 10.55% Sn alloy (Figure 4b) at which point an acicular phase, the intermetallic compound FeSn, appears (Figure 4c). Figure 7 shows the solid solution hardening produced in ferrite by the presence of tin. The low- and medium-carbon series (Figures 5 and 6) show the presence of an acicular phase, suggestive of FeSn, already at concentrations less than 3% Sn (see, for example, Figure 6b), although there is reason to believe it is neither FeSn nor cementite but rather a ternary carbide.

23. HANSEN, M., and ANDERKO, K. *Constitution of Binary Alloys.* McGraw-Hill, New York, 2nd ed., 1959.

Table 1. Fe-Sn AND Fe-Sn-C ALLOYS

Alloy No.	Composition %C	Composition %Sn	Electron Probe Analysis (%Sn) Ferrite Matrix	Carbide	Intermetallic Phase (FeSn)	Overall	Carbide Extract %C	Carbide Extract %Sn	Ferrite Lattice Parameter†	
A-1	0.01	-							2.8665	
A-2	0.02	3.39							2.8785	M=0.003707
A-3	0.01	6.61							2.8905	
A-4	0.01	10.55							2.9055	
A-5	0.01	13.65	14.0	-	-	-			2.9149	
A-6	0.01	17.45	17.3	-	23.8*	-			2.9167	
A-13	0.01	22.10							[illegible]	(400°C)
									[illegible]	(600°C)
									[illegible]	(800°C)
									[illegible]	(900°C)
A-7	0.28								2.8665	
A-8	0.27	3.47	3.5	11.6-19.2*		4.6	5.3	23.2	2.8732	M'=0.002043
A-9	0.26	6.98	6.1	11.9*		9.1	6.6	35.5	2.8809	k=21.4
A-10	0.24	10.21	7.6	13.3*	23.7*	11.6	2.3	52.4	2.8882	
A-11	0.21	13.53	9.4	16.6*	44.0-61.7*	18.7			2.8896	
A-12	0.15	17.22							2.8886	
A-15	0.52	0.89							2.8675	k=31.6
A-16	0.48	2.79							2.8707	M'=0.001593
A-17	0.45	8.45							2.8800	k=20.0
A-18	0.42	12.39					2.8	41.1	2.8861	k=23.3
A-19	0.42	16.93							2.8892	

†Annealed at 600 C unless otherwise indicated
*Includes excitation of adjacent areas

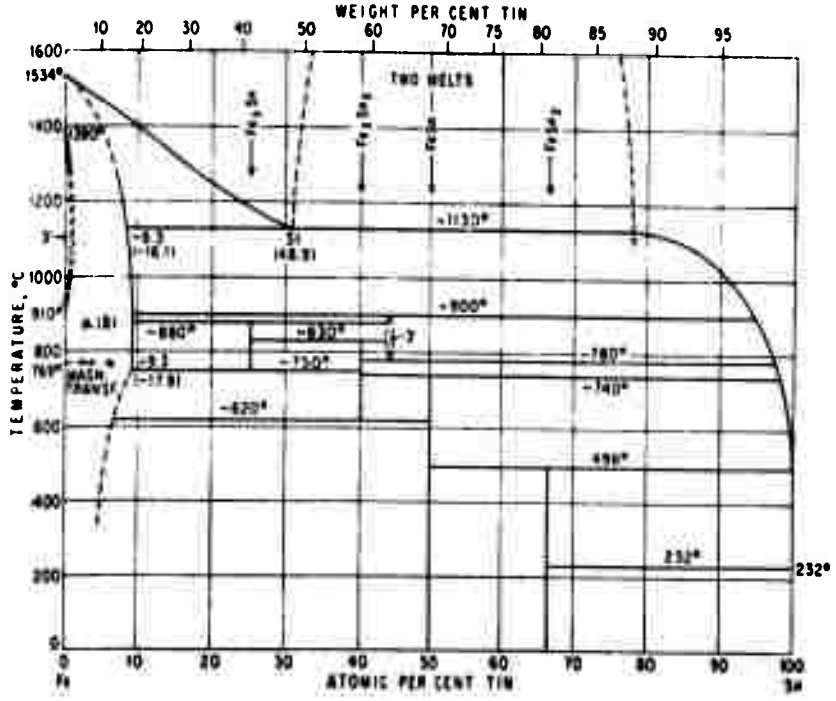

Figure 3. Iron-tin binary phase diagram (Reference 23).
(Courtesy of McGraw-Hill Company)

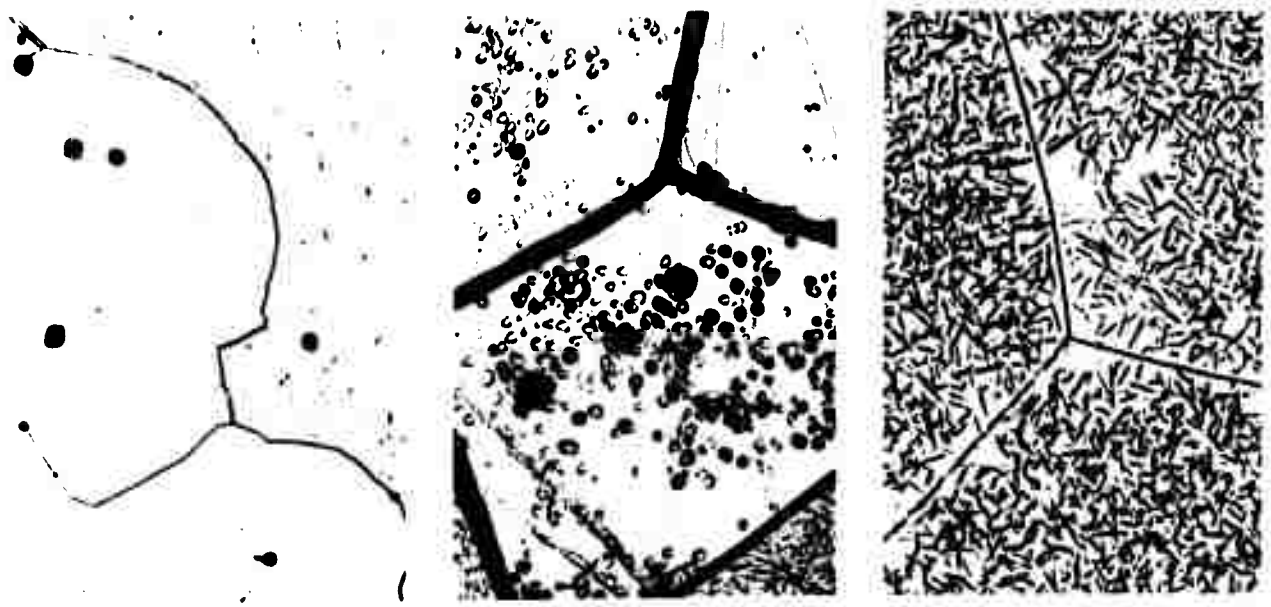

a. Fe-3.39%Sn b. Fe-10.66%Sn c. Fe-13.65%Sn

Figure 4. Microstructures of alloys of the Fe-Sn binary series (%C∿0.02). Mag. 500X.

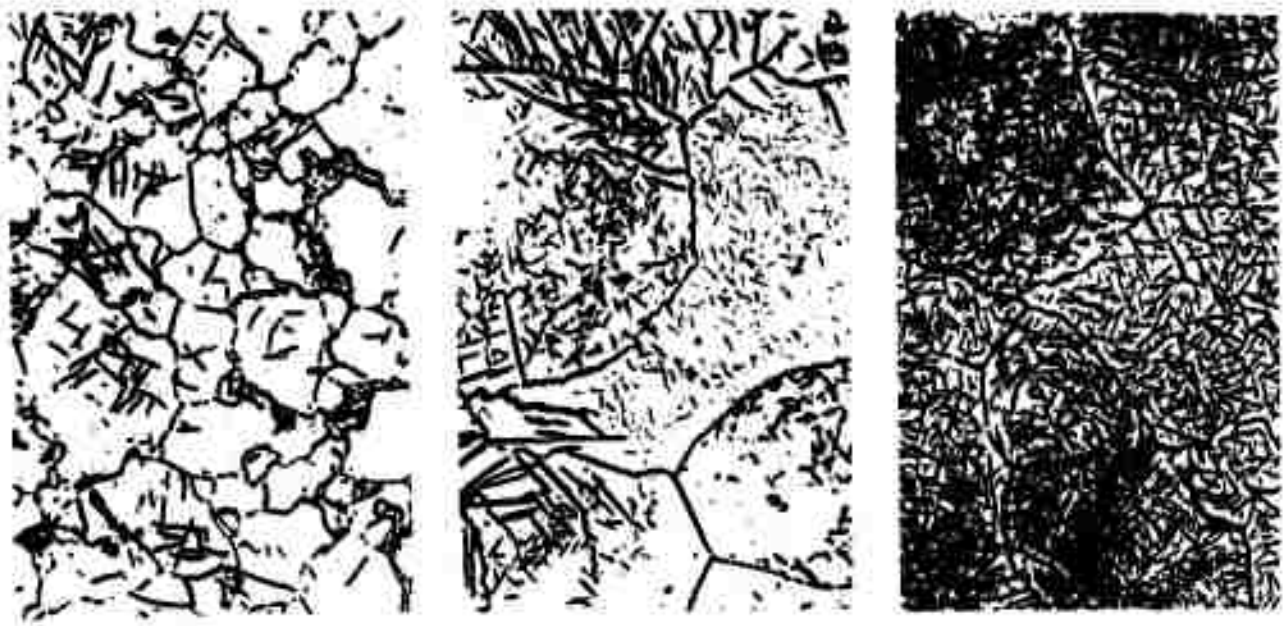

a. Fe-3.47%Sn-0.27%C b. Fe-10.21%Sn-0.24%C c. Fe-13.53%Sn-0.21%C

Figure 5. Microstructures of Fe-Sn-C alloys of the low-carbon series. Mag. 500X.

a. Fe-0.89%Sn-0.52%C

b. Fe-2.79%Sn-0.48%C

c. Fe-12.39%Sn-0.42%C

d. Fe-16.93%Sn-0.42%C

Figure 6. Microstructures of Fe-Sn-C alloys of the medium-carbon series. Mag. 500X.

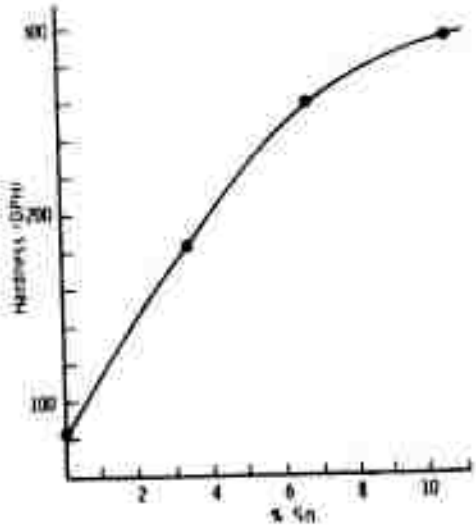

Figure 7. The hardening of ferrite by tin.

Some representative results obtained by electron microprobe analysis are presented in Table 1. Two tin-rich phases were encountered in the alloys; that phase showing the highest concentration of tin is most likely FeSn, the other a tin-bearing carbide. The FeSn compound is not encountered below approximately 10 wt% Sn in any of the alloys. One further notices that in all carbon-bearing alloys the tin content of the ferrite matrix is below that of the alloy as a whole (when measured by the microprobe), and that all carbides were observed to be richer in tin than the matrix. The concentrations reported for the carbides should not be taken to be quantitative since areas of the adjacent matrix were also excited by the electron beam and so contributed to the measured fluorescent intensities. Nevertheless, the results point indisputably toward the conclusion that there is an enrichment of the carbide phase in tin and a corresponding depletion of the ferrite matrix.

The chemical analyses of the extracted carbides agree reasonably well with the microprobe results, in that every case shows an enrichment of the carbide in tin by a factor of approximately 3 to 6. These results are also presented in Table 1. However, one must be extremely cautious in evaluating these results quantitatively in view of the many technical difficulties associated with this technique. For example, the dissolution of tin from the matrix and its undetected reprecipitation on the carbide extract, or the reverse problem of the dissolution of tin from the carbide would both lead to errors in the subsequent chemical analysis which are difficult to detect and evaluate.

Table 2 presents X-ray diffraction data obtained from carbides extracted from alloys of the medium-carbon series. These are compared with diffraction results obtained from cementite (Fe_3C) extracted from a binary Fe-C alloy and with the ASTM diffraction standards for Fe_3C. The peaks were indexed assuming the carbide to be of the $(FeSn)_3C$ type having an orthorhombic crystal structure. The calculated orthorhombic lattice parameters are shown plotted versus the tin concentration *of the alloy* in Figure 8. Since the atomic radius of tin exceeds that of iron, one would expect that the substitution of tin for iron on the orthorhombic lattice will result in an increase in unit cell dimensions. The fact that the calculated lattice parameters are larger in the higher tin alloys therefore suggests a higher tin content for the carbide. However, the fact that the parameters fail to show a smooth increase throughout the entire range of alloy compositions points to the possibility that a phase boundary has been reached and that a different carbide phase has formed.

The large standard deviations found with the carbide lattice parameters from the higher tin alloys support this view in that the diffraction data are poorly described by a set of orthorhombic lattice parameters. It was found that many of

Table 2. X-RAY DATA FROM CARBIDES EXTRACTED FROM Fe-Sn-C ALLOYS

hkl	Fe_3C (ASTM Standard)	Alloy A-7 0%Sn	A-15 0.89%Sn	A-16 2.79%Sn	A-17 8.45%Sn	A-18 12.39%Sn	A-19 16.93%Sn
020	2θ = I = VW† d = 2.54		55.167 -M 2.474	55.100 M 2.477	-	-	-
112/021	2θ = I = VS d = 2.38		57.266 S 2.390	-	-	-	-
200	2θ = I = M d = 2.26	60.433 M 2.276	60.737 -M 2.266	61.017 VS 2.256*	61.233 VS 2.249*	61.366 VS 2.245*	61.466 VS 2.242*
120	2θ = I = M d = 2.23	-	62.067 -M 2.222	62.500 VW 2.208	-	62.333 -W 2.213	62.500 -M 2.208
121	2θ = I = VS d = 2.10	65.444 VS 2.119	65.733 S 2.111	-	-	65.969 VW 2.104	66.067 VW 2.101
210	2θ = I = VS d = 2.06	-	67.167 S 2.071	-	-	-	67.770 -W 2.055
103	2θ = I = VS d = 2.01	-	69.233 VS 2.016	69.000 VW 2.022	-	69.667 VW 2.006	69.767 +W 2.003
211	2θ = I = VS d = 1.99	70.432 VS 1.986	70.700 S 1.980	71.911 S 1.951*	72.150 VS 1.945*	72.266 VS 1.943*	72.333 S 1.941*
113	2θ = I = -M d = 1.87	-	75.346 +M 1.874	-	-	-	-
122	2θ = I = S d = 1.86	-	76.233 -S 1.856	-	-	-	-
212	2θ = I = -M d = 1.77	- -	80.978 +W 1.764	82.599 +W 1.736*	82.433 -M 1.739*	82.520 -M 1.737*	82.599 +W 1.736*
004/023	2θ = I = -M d = 1.68	-	85.555 -M 1.687	-	-	-	-
221	2θ I = -W d = 1.61	-	88.455 W 1.642	-	-	-	-
130	2θ = I = -M d = 1.59	91.933 -M 1.593	92.200 +W 1.590	92.200 W 1.590*	92.473 M 1.586*	92.533 M 1.585*	92.633 W 1.584*
222	2θ = I = W d = 1.51	98.266 W 1.515	98.811 +W 1.509	98.235 -W 1.515	-	-	98.967 VW 1.507
033	2θ = I = d =		112.815 VW 1.375	112.767 -S 1.376*	113.147 VS 1.373*	113.155 VS 1.373*	113.233 -S 1.372*
320	2θ = I = d =		124.770 VW 1.293*	124.233 -W 1.296*	124.599 -M 1.294*	124.599 W 1.294*	124.711 VW 1.293*
322	2θ = I = d =		138.400 +M 1.225*	137.333 -M 1.230*	137.933 -M 1.227*	138.067 +W 1.227*	138.133 W 1.227*

†Intensities: S = strong, M = medium, W = weak, V = very
*These d-spacings may also be indexed as cubic reflections in the order (111), (200), (210), (211), (220), (221)/(300), (310).

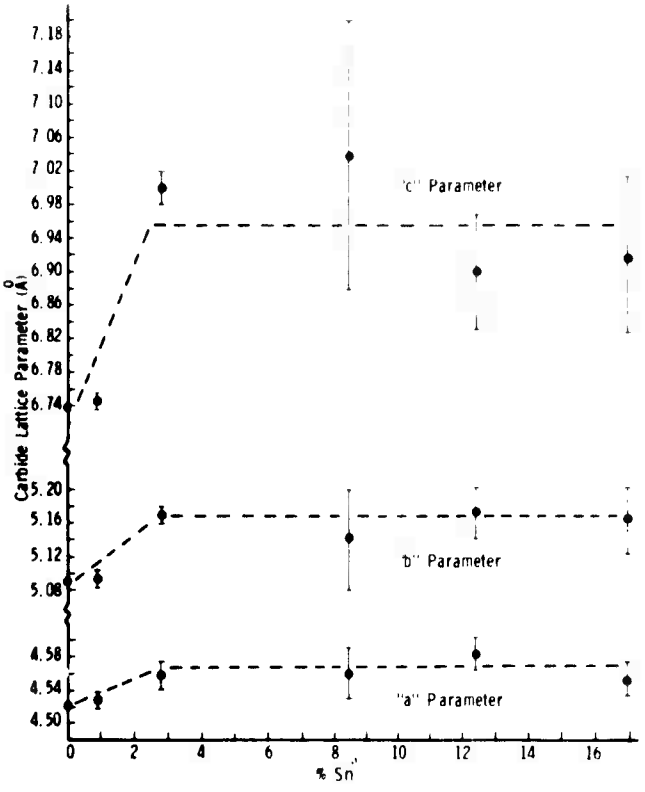

Figure 8. Lattice parameters of orthorhombic $(FeSn)_3C$ as a function of tin concentration in Fe-Sn-C alloys of the medium-carbon series.

the diffraction peaks obtained from Specimens A-16 through A-19 were also consistent with the diffraction pattern obtained from a cubic crystal with a lattice parameter of 3.88 Å (cf. Table 3). The metallographic and X-ray investigations of Stadelmaier and coworkers[24,25] did in fact report the presence at 800 C of a ternary carbide having an ordered cubic crystal structure with a lattice parameter of 3.86 Å, with a composition variously reported as Fe_3SnC or $Fe_{70}Sn_{15}C_{15}$. It would thus appear that the extracted carbide specimens may have been a mixture of this ternary carbide with another phase, most likely cementite. No evidence for a contribution from the FeSn phase to the observed diffraction patterns was found.

What probably constitute the most precise data relating to phase relations in the Fe-Sn-C system are the ferrite lattice parameter measurements. These data are shown in Table 1 and also appear plotted versus tin concentration in Figure 9. The lattice parameters for the Fe-Sn binary alloys agree well with previously reported results,[26] showing the ferrite lattice to be expanded as expected by the substitution of the larger tin atom. One binary alloy (Specimen A-13) was annealed at a variety of temperatures within the two-phase field; its lattice parameters define the solubility limit for tin in ferrite at these temperatures. The measured solvus line is shown on the binary phase diagram in Figure 10. The solubilities at 800 and 900 C agree with published values based upon the metallographic work of Edwards and Preece;[27] agreement is not as good with the X-ray study of Ehret and Westgren.[26] The lower temperature values have not before been measured.

From Figure 9, the fact that M' for the Fe-Sn-C alloys is less than M for the Fe-Sn binary alloys indicates immediately that the distribution coefficient k is greater than one, and that the element Sn partitions to the carbide phase, qualitatively corroborating all previous observations in this study. The values of k calculated from Equation (9), when the alloys were grouped into low- and medium-carbon series, are presented in Table 1. The very large values of k indicate a steeply sloping tie line in the "ferrite + carbide" two-phase field

24. STADELMAIER, H. H., and HUETTER, L. L. *Ternary Carbides of the Transition Metals Nickel, Cobalt, Iron, Manganese with Zinc and Tin.* Acta Met., v. 9, 1959, p. 415-419.
25. STADELMAIER, H. H., and WALLER, J. M. *Über das ternäre System Eisen-Zinn-Kohlenstoff.* Metall., v. 15, 1961, p. 125-126.
26. EHRET, W. F., and WESTGREN, A. F. *X-Ray Analysis of Iron-Tin Alloys.* J. Am. Chem. Soc., v. 55, 1933, p. 1339-1351.
27. EDWARDS, C. A., and PREECE, A. *A Study of the Constitution of the Iron-Tin Alloys.* J. Iron Steel Inst., v. 124, 1931, p. 41-66.

Table 3. Fe-P AND Fe-P-C ALLOYS

Alloy No.	Composition %C	Composition %P	Electron Probe Analysis (% P) Ferrite Matrix	Carbide	Intermetallic Phase (Fe_3P)	Overall	Carbide Extract %P	Ferrite Lattice Parameter+
B-2	0.02	0.69	. . . . .					2.8659
B-1	0.02	1.37	. . . . .					-
B-3	0.02	2.08	. . . . .					-
B-4	0.02	2.65	2.29	-	15.3	-	. . . .	-
B-5	0.02	3.31	2.07	-	15.3	-	. . . .	-
B-6	0.31	0.68	0.78-1.96	0.26-0.73*	-	0.75	5.6	2.8663
B-7	0.32	1.41	1.39-1.81	1.40	-	1.57	10.9	2.8664
B-8	0.31	1.98	. . . . .				16.4	2.8662
B-9	0.28	2.16	2.08-2.55	0.63*	15.1	2.65	13.9	2.8664
B-10	0.31	2.85	1.05-2.40	3.45*	15.2	4.38	13.5	2.8664

+Annealed at 600 C
*Includes excitation of adjacent area

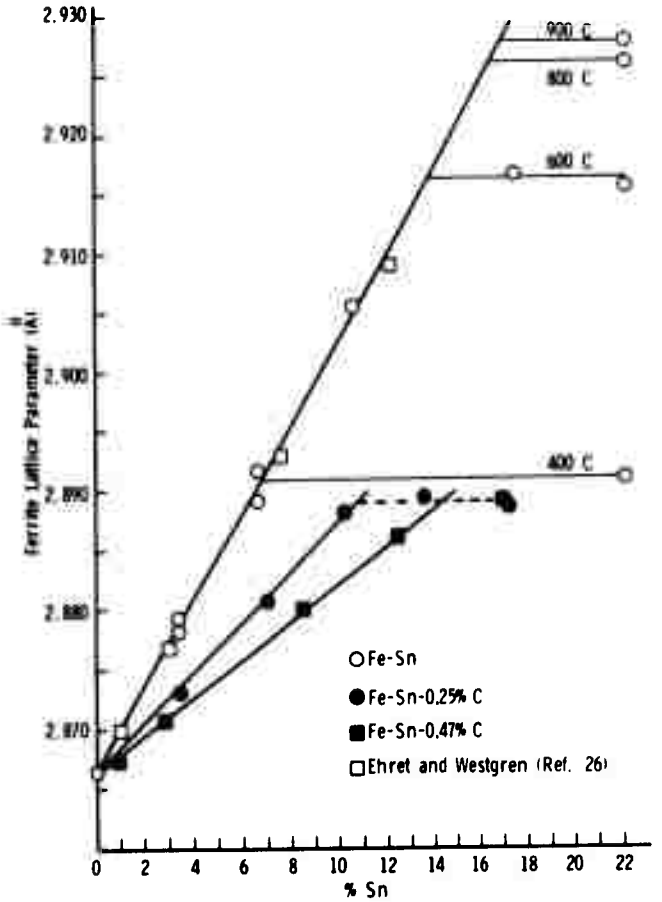

Figure 9. Ferrite lattice parameter as a function of tin concentration in Fe-Sn and Fe-Sn-C alloys, annealed at 600 C unless otherwise indicated.

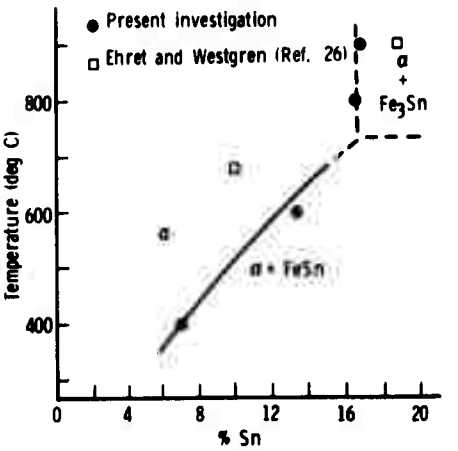

Figure 10. Iron-rich end of the iron-tin binary phase diagram based upon present results, showing the α-solvus.

(i.e., a steep slope opposite to that in Figure 2), requiring the existence of a tin-rich ternary carbide, probably not of the cementite structure. It would appear in fact that the two-phase field being traversed by the low- and medium-carbon series of alloys is not the "ferrite + cementite" field, but rather the "ferrite + ternary carbide" two-phase field, and that the isothermal section through the ternary phase diagram must appear as illustrated in Figure 11. Such a diagram would be consistent with the higher temperature isothermal sections reported by Stadelmaier and coworkers.[25] Because the carbon content of the ternary carbide is different from that of cementite, the distribution coefficients calculated from Equation (9) and reported in Table 1 should in reality be approximately 30 percent lower, but they nevertheless remain considerably larger than one. Unfortunately, the limited extent of the "ferrite + cementite" two-phase field if it is indeed as shown in Figure 11, would not allow a determination of the distribution coefficient for tin between these latter two phases.

Fe-P and Fe-P-C Alloys

The published Fe-P binary phase diagram[23] is shown in Figure 12. The alloy series containing phosphorus is divided into two groups (see Table 3): (1) a binary Fe-P series (%C∿0.02) and (2) a medium-carbon series (%C∿0.31). The microstructures of alloys which were homogenized at 900 C and annealed at 600 C for two weeks are shown in Figures 13 and 14. A second phase (Fe_3P) appears in the binary alloys containing more than 1 wt% P, in agreement with the early metallographic work of Vogel and Bauer[28] and consistent with the published phase diagram. However, Fe_3P was not detected in the ternary Fe-P-C alloys by the electron microprobe until phosphorus concentrations in excess of 2 wt% were reached. The solid solution hardening of ferrite due to substitutionally dissolved phosphorus is indicated in Figure 15, but unfortunately only one data point occurs in what is most probably the single-phase ferrite region.

The electron microprobe results shown in Table 3 are generally inconclusive. One is unable to say whether or not the phosphorus content of the ferrite matrix is depleted in those ternary alloys in which only carbides have formed. Once Fe_3P begins to form, however, the matrix is clearly depleted of phosphorus, as one would expect.

The chemical analyses of "carbides" extracted from several Fe-P-C alloys of the medium-carbon series are also presented in Table 3. The results for the three alloys with phosphorus contents of 2 wt% and above (B-8, B-9, and B-10) most likely represent the analysis of what is predominantly the phosphide Fe_3P. There is an apparent enrichment of the carbide in the lower phosphorus alloys, although these results also may be influenced by contamination by a similar phosphide phase. The ferrite lattice parameter measurements tend to confirm the interpretation that a true enrichment of the carbide has in fact occurred, however.

The early X-ray work of Hägg[29] on iron-phosphorus alloys detected no change in the ferrite lattice parameter due to phosphorus, in spite of the atomic radius

28. VOGEL, R., and BAUER, H. *The Ternary System: Iron-Nickel-Phosphorus.* Arch. Eisenhüttenw., v. 5, 1931, p. 269-278.
29. HÄGG, G. *X-Ray Studies of the Binary Systems of Iron with Phosphorus, Arsenic, Antimony, and Bismuth.* Z. Krist., v. 68, 1928, p. 470-472.

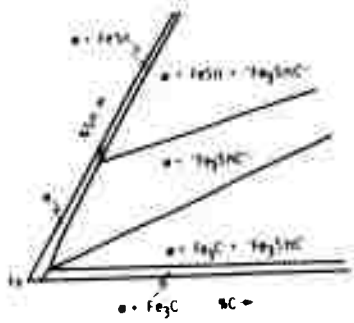

Figure 11. Schematic representation of the Fe-Sn-C ternary phase diagram at 600 C consistent with the present experimental data.

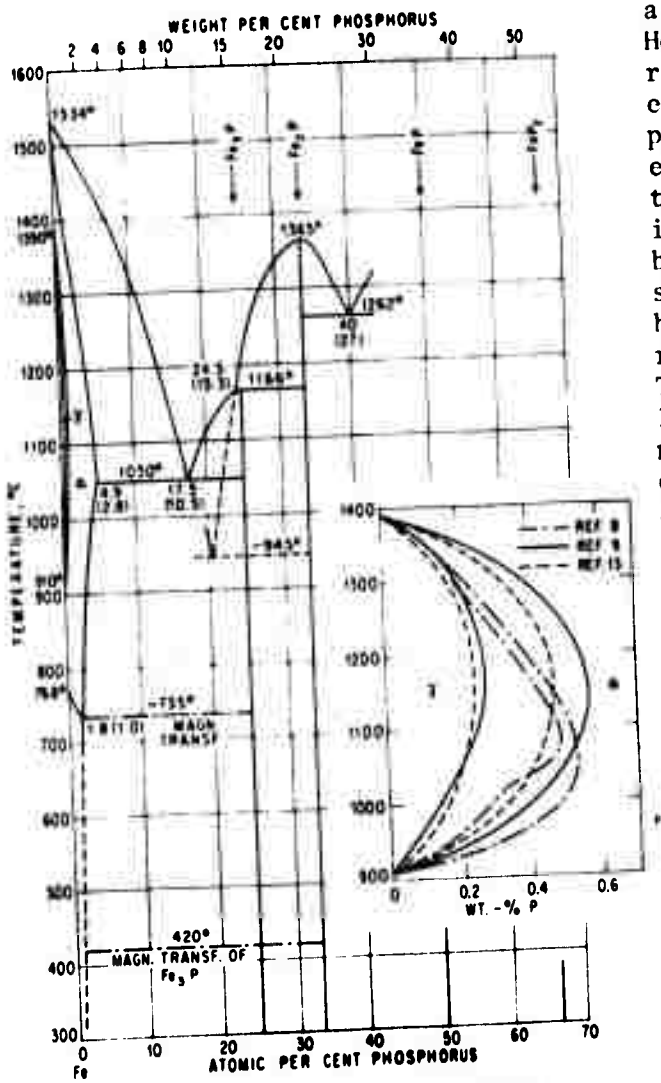

Figure 12. Iron-phosphorus binary phase diagram (Reference 23). (Courtesy of McGraw-Hill Company)

of phosphorus being less than that of iron. Hornbogen[30] and later Gale,[31] however, observed a decrease in the lattice parameter measured in alloys quenched from 1100 C, indicating that phosphorus dissolves substitutionally in ferrite. The results of the present study on annealed alloys are presented in Table 3 and are plotted versus phosphorus content in Figure 16. Meaningful lattice parameter results were not obtained from the higher phosphorus binary alloys, due possibly to a lack of homogeneity in these specimens. However, the lattice parameter in the single-phase binary alloy (0.69% P) appears to support Hornbogen's and Gales' findings. The results from the ternary Fe-P-C alloys exhibit a lesser reduction in lattice parameter due to phosphorus than that experienced by the binary alloys, with the solubility limit occurring roughly in the vicinity of 1 wt% P. This solubility limit is somewhat below that suggested by the microprobe results but appears more consistent with the results from the binary alloy series. The relative changes in the ferrite lattice parameter in binary and ternary alloys point toward a partitioning of phosphorus to the carbide phase and a depletion of the ferrite matrix, resulting in a distribution coefficient k greater than one. A quantitative calculation of k from Equation (10) was not considered warranted by the data, however. Nevertheless, this qualitative result is consistent with the conclusion drawn from the extracted carbide analyses.

30. HORNBOGEN, E. *Precipitation of Phosphorus from Alpha-Iron and Its Effect on Plastic Deformation.* Trans. ASM, v. 53, 1961, p. 569-588.

31. GALE, B. *Lattice Parameters of Solid Solutions of Phosphorus in Iron.* Acta Met., v. 7, 1959, p. 420-421.

a. Fe-0.69%P

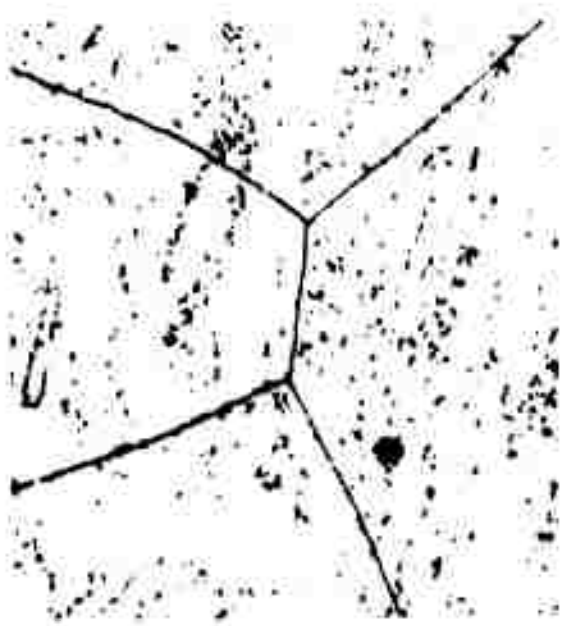

b. Fe-1.37%P

c. Fe-2.08%P

d. Fe-3.31%P

Figure 13. Microstructures of alloys of the Fe-P binary series (%C≈0.02). Mag. 500X.

a. Fe-0.68%P-0.31%C

b. Fe-1.41%P-0.32%C

c. Fe-2.16%P-0.28%C

d. Fe-2.85%P-0.31%C

Figure 14. Microstructures of Fe-P-C alloys of the medium-carbon series. Mag. 500X.

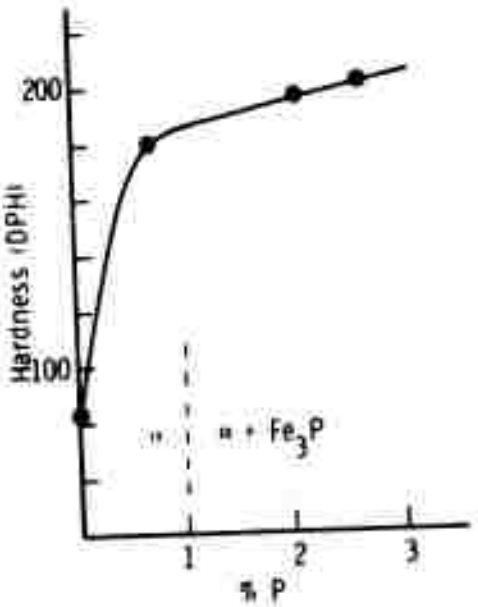

Figure 15. The hardness of Fe-P alloys showing the solid solution hardening of ferrite by phosphorus.

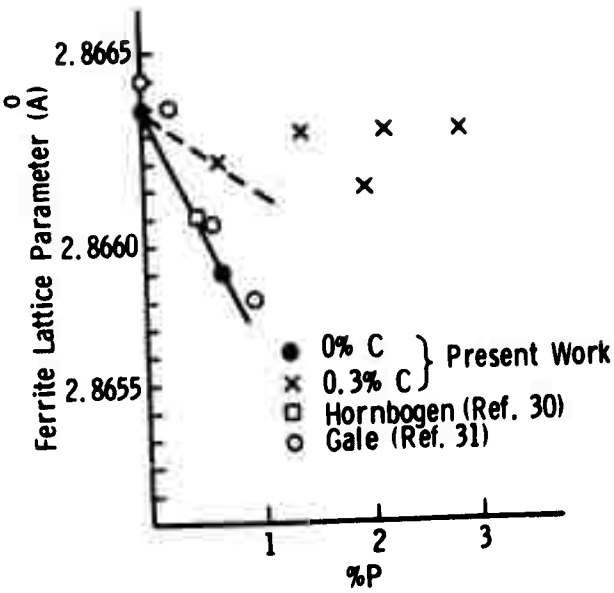

Figure 16. Ferrite lattice parameter as a function of phosphorus concentration in Fe-P and Fe-P-C alloys, annealed at 600 C.

Fe-Si and Fe-Si-C Alloys

The published Fe-Si binary phase diagram[23] is shown in Figure 17. The alloy series containing silicon may be subdivided into (1) a binary Fe-Si series (%C∿0.02) and (2) a medium-carbon series (%C∿0.38; see Table 4). The microstructures of alloys homogenized at 900 C and annealed two weeks at 600 C are shown in Figures 18 and 19. The ordered α' phase in this alloy system does not manifest itself in any microstructural change although the presence of ordered α' is clearly evidenced in the lattice parameter measurements discussed later. The solubility limit of the homogeneous ferrite phase has been reached in Figure 18b, where the first evidence of the ε-phase (FeSi) appears. The solid solution hardening of ferrite by silicon (in both disordered α and ordered α') is shown in Figure 20. The medium-carbon series in Figure 19 shows the presence of carbides in all the microstructures, but FeSi is not encountered. Neither was the presence of FeSi ever detected by the electron microprobe analyses of the ternary alloys. Thus, the solubility limit of silicon in the ferrite of the medium-carbon alloys apparently was never exceeded.

The electron microprobe results are presented in Table 4. The direct analysis of the silicon concentration in the carbides again could not be made due to the unavoidable excitation of the adjacent ferrite matrix. However, the concentration of silicon in the matrix was consistently shown to be greater than that of the overall alloy, pointing to an enrichment of the ferrite and a corresponding depletion of the carbide of silicon. The distribution coefficient k should, therefore, be less than one, and in fact is found to be less than one in the X-ray results.

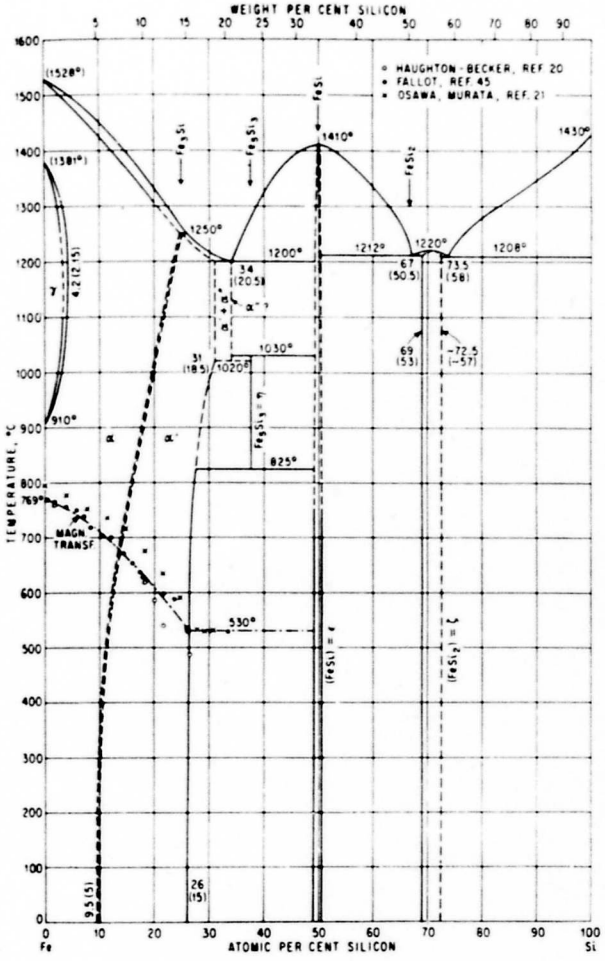

Figure 17. Iron-silicon binary phase diagram (Reference 23). (Courtesy of McGraw-Hill Company)

Table 4. Fe-Si AND Fe-Si-C ALLOYS

Alloy No.	Composition %C	Composition %Si	Electron Probe Analysis (% Si): Ferrite Matrix	Carbide	Intermetallic Phase (FeSi)	Overall	Carbide Extract %C	Carbide Extract %Si	Ferrite Lattice Parameter†	
C-1	0.01	3.50	. . . . .				. . . . .		2.8622	
C-2	0.01	7.01	. . . . .				. . . . .		2.8521	
C-3	0.03	10.31	. . . . .				. . . . .		2.8414	M=-0.002968
C-12	0.02	14.60	. . . . .				. . . . .		2.8295	
C-13	0.02	17.90	. . . . .				. . . . .		2.8251	
C-14	0.01	21.00	. . . . .				. . . . .		2.8264	
C-6	0.38	-	. . . . .				. . . . .		2.8666	
C-7	0.38	3.52	2.97-3.17	2.73-3.04*	-	3.10	3.4	4.0	2.8622	
C-8	0.38	6.94	6.58-7.65	-	-	6.57	4.9	2.7	2.8519	M'=-0.003131
C-9	0.38	10.46	9.80-10.20	7.26*	-	8.05	4.9	3.4	2.8408	k=0.064
C-15	0.34	13.90	14.4	13.8*	-	14.1	. . . . .		2.8294	

†Annealed at 600 C
*Includes excitation of adjacent areas

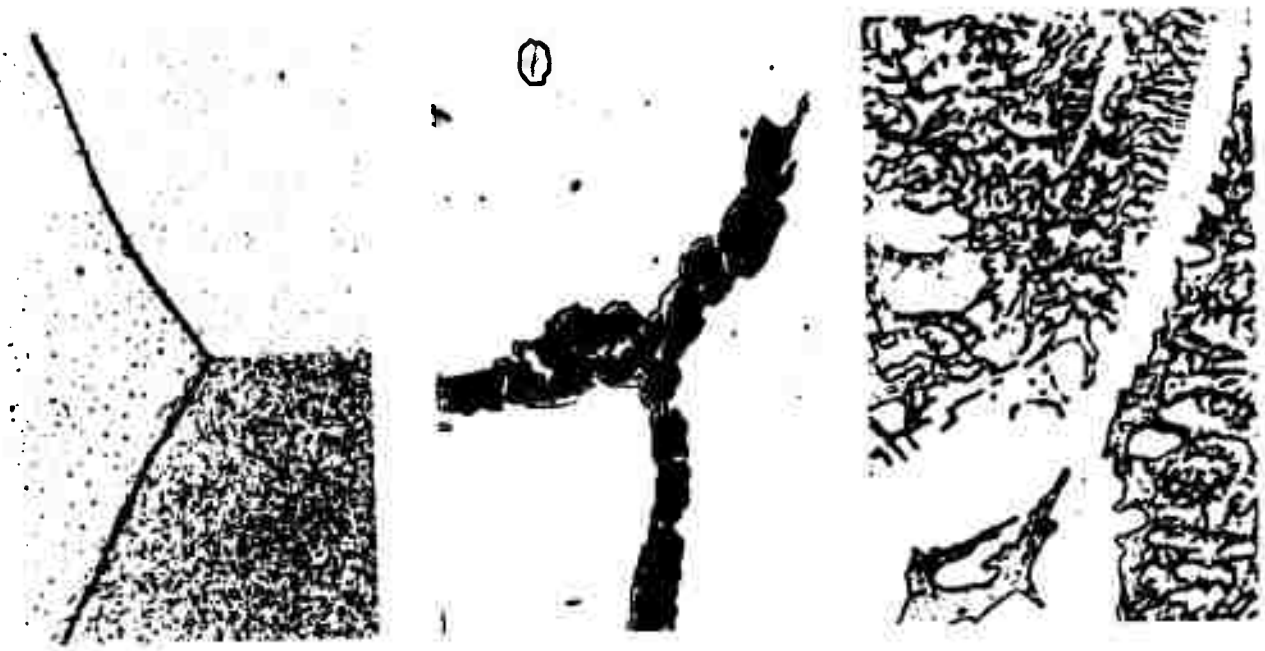

a. Fe-3.50%Si b. Fe-17.90%Si c. Fe-21.00%Si

Figure 18. Microstructures of alloys of the Fe-Si binary series (%C∿0.02). Mag. 500X.

Table 4 also presents the results of the chemical analyses of carbides extracted from the ternary Fe-Si-C alloys. In spite of the inherent technical difficulties associated with this technique, it was possible to demonstrate that the carbide phase invariably has a lower silicon concentration than the alloy as a whole, indicating a depletion of the carbide consistent with the other measurements. The results of other workers also support this view. Owen[32] measured the lattice parameters of carbides extracted from Fe-Si-C alloys and found no difference from the parameters of Fe_3C, suggesting very little solubility of silicon in the carbide phase. In addition, the analysis of carbides extracted from a 1.66% Si-0.69% Mn-0.51% C steel by Kuo[17] also showed a depletion of silicon in the carbide.

The ferrite lattice parameter measurements are presented in Table 4 and are plotted versus silicon concentration in Figure 21. The data agree well with the earlier work of Jette and Greiner[33] (not plotted), Farquhar et al,[34] and Lihl and Ebel.[35] The sharp break in the lattice parameter plot near 6 wt% Si indicates the composition at which the ordered α' phase begins to form. The break in the plot beyond 15 wt% Si indicates the solubility limit in ferrite. Both of these values agree with published phase diagram data.[23]

32. OWEN, W. S. *The Carbide Phase in Iron-Carbon-Silicon Alloys.* J. Iron Steel Inst., v. 167, 1951, p. 117-120.
33. JETTE, E. R., and GREINER, E. S. *An X-Ray Study of Iron-Silicon Alloys.* Trans. AIME, v. 105, 1933, p. 259-274.
34. FARQUHAR, M. C. M., LIPSON, H., and WEILL, A. R. *An X-Ray Study of Iron-Rich Iron-Silicon Alloys.* J. Iron Steel Inst., v. 152, 1945, p. 457-472.
35. LIHL, F., and EBEL, H. *Röntegenographische Untersuchungen über den Aufbau eisenreicher Eisen-Silizium-Legierungen.* Arch. Eisenhüttenw., v. 32, 1961, p. 489-491.

a. Fe-3.52%Si-0.38%C

b. Fe-6.94%Si-0.38%C

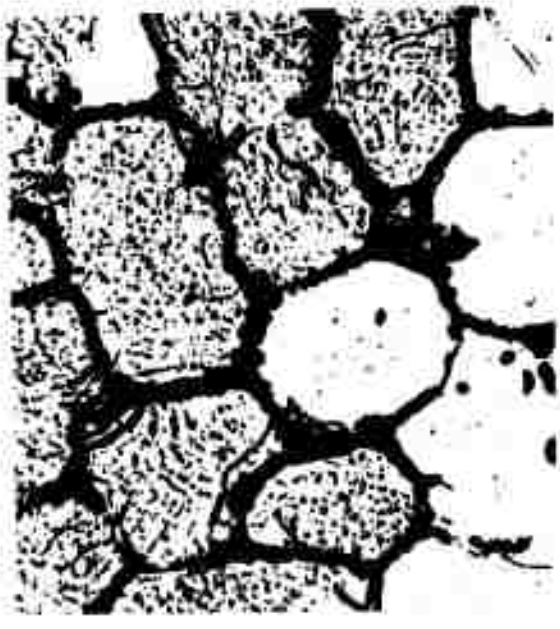

c. Fe-10.46%Si-0.38%C

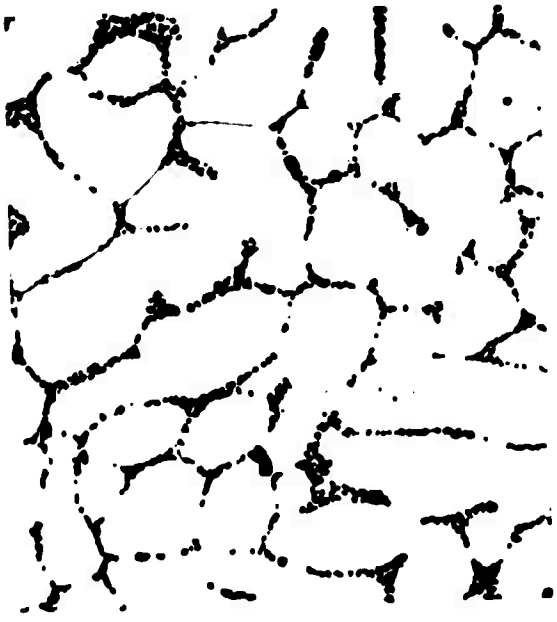

d. Fe-13.90%Si-0.34%C

Figure 19. Microstructures of Fe-Si-C alloys of the medium-carbon series. Mag. 500X.

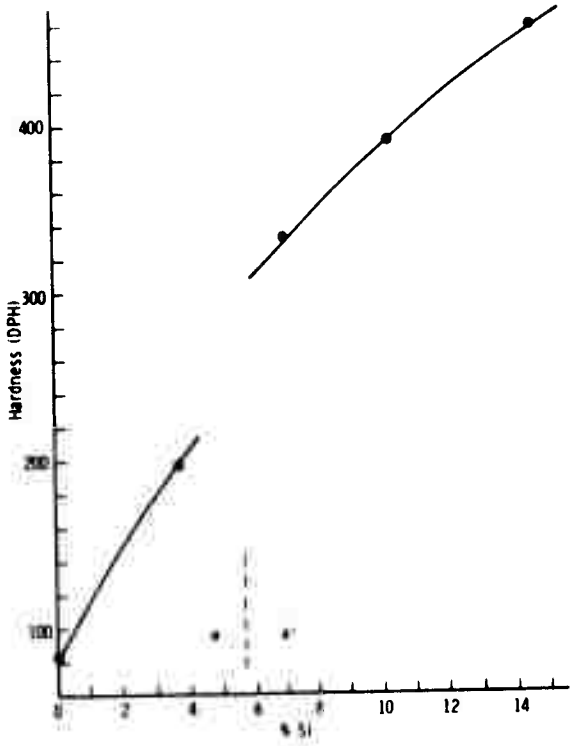

Figure 20. The hardness of Fe-Si alloys showing the solid solution hardening of α and α' by silicon.

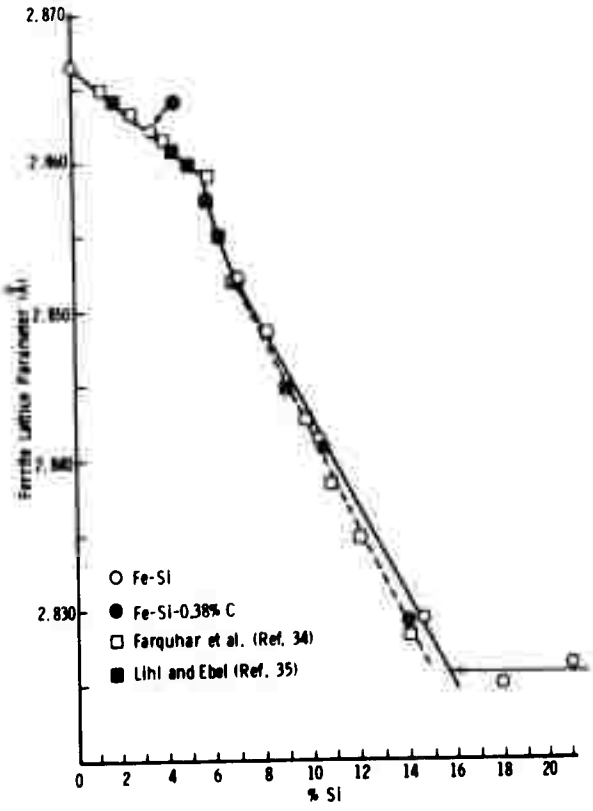

Figure 21. Ferrite lattice parameter as a function of silicon concentration in Fe-Si and Fe-Si-C alloys, annealed at 600 C.

The amount of current data is limited and does not permit the accurate determination of the slopes of the two segments of the plot in Figure 21. In the disordered α region, M for the binary alloys and M' for the ternary alloys cannot be distinguished. In the ordered α' region, however, $|M'|$ is clearly greater than $|M|$, indicating a distribution coefficient k of less than one. Calculating the distribution coefficient from Equation (9)* gave $k \sim 0.6$, in general agreement with the electron microprobe and carbide extract results. These results, of course, pertain to the equilibrium between ordered α' and carbide, but hopefully they do not differ much from the desired α/carbide equilibrium relations.

Fe-Sb and Fe-Sb-C Alloys

The published Fe-Sb binary phase diagram[23] is shown in Figure 22. By far the greatest amount of effort was expended in investigating this particular alloy system and the most contradictory results were obtained. The alloy series may be subdivided into four groups (see Table 5): (1) a binary Fe-Sb series (%C$\sim$0.02), (2) a low-carbon series (%C$\sim$0.12), (3) a medium-carbon series (%C$\sim$0.35), and (4) a high-carbon series (%C$\sim$0.53). The microstructures of several of these alloys homogenized at 900 C and annealed at 600 C are shown in Figures 23 to 25. Figure 23 presents a series of binary alloys with increasing antimony contents. The

*Equation (9) could be used directly on the data from the α' region because the lattice parameter intercept at 0% Si (i.e., a(o)) fortuitously turned out to be the same for both the binary and the ternary alloys.

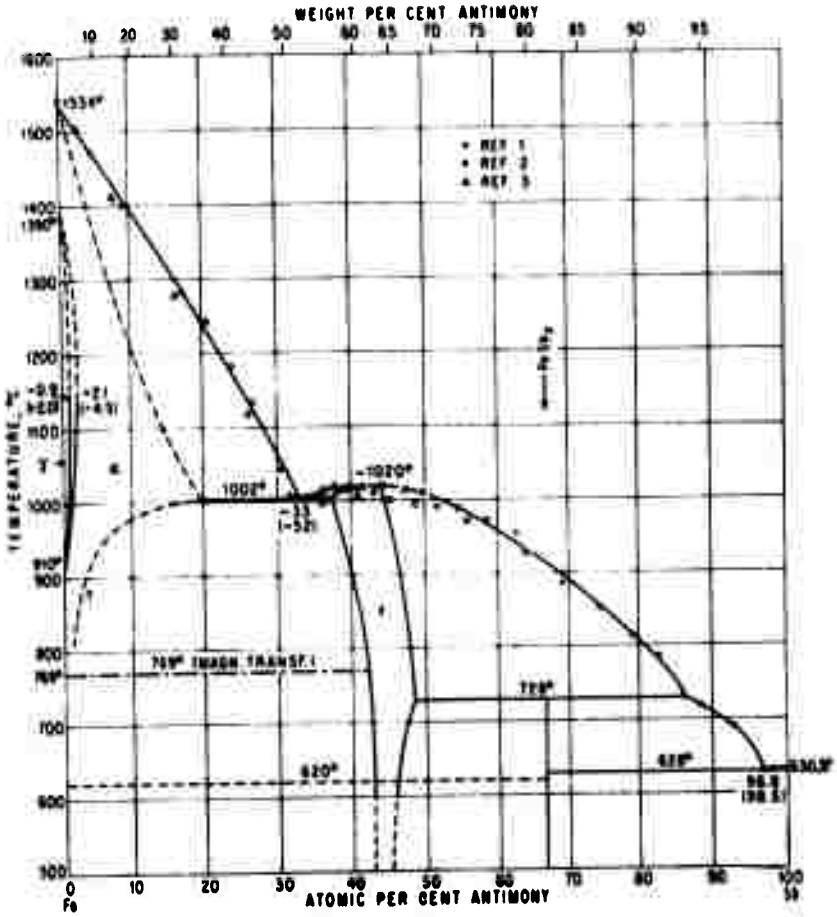

Figure 22. Iron-antimony binary phase diagram (Reference 23). (Courtesy of McGraw-Hill Company)

solubility of antimony in ferrite is not exceeded until a concentration of roughly 5 wt% Sb is reached (Figure 23c), at which point the ε-phase (Fe_3Sb_2) is observed. The solid solution strengthening of ferrite by antimony is illustrated by the hardness data plotted in Figure 26.

Figure 24 shows the microstructures of the alloys of medium-carbon series. Here the ε-phase is already observed at 2.80 wt% Sb (Figure 24b) suggesting that the solubility of the ε-phase in ferrite is markedly reduced in the presence of carbon. There is little ambiguity in distinguishing the ε-phase from cementite in these alloys because, under polarized light, ε appears bright red whereas cementite appears bluish in color. However, this reduced solubility of the ε-phase is not observed in the higher carbon alloys, nor is it corroborated by the ferrite lattice parameter measurements. The metallographic results are also inconsistent with the X-ray results in other ways to be discussed later, forcing one to speculate that these are not, in fact, phases in equilibrium in these medium-carbon alloy microstructures. The appearance of the cementite in pearlite colonies indicates that austenite was formed during the homogenizing heat treatment at 900 C. It may be that the ε-phase also formed at this temperature and then, for kinetic reasons, did not dissolve during the 600 C anneal, but this interpretation is only speculative.

a. Fe-0.49%Sb

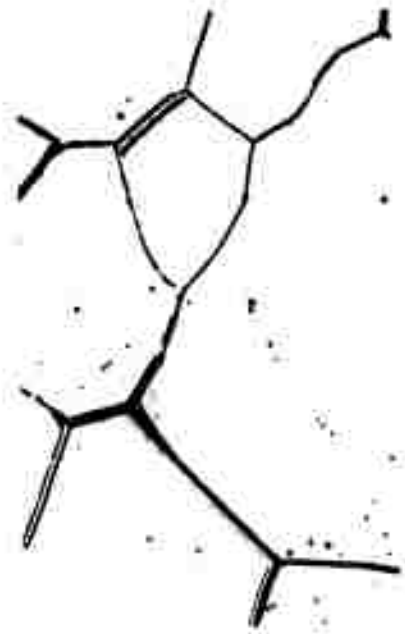

b. Fe-1.94%Sb

c. Fe-5.54%Sb

d. Fe-15.10%Sb

Figure 23. Microstructures of alloys of the Fe-Sb binary series (%C~0.02). Mag. 500X.

a. Fe-1.45%Sb-0.36%C

b. Fe-2.80%Sb-0.35%C

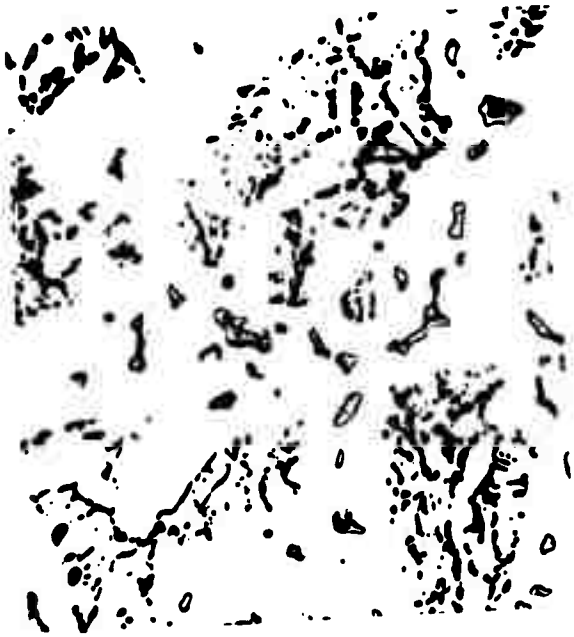

c. Fe-4.04%Sb-0.35%C

d. Fe-5.48%Sb-0.36%C

Figure 24. Microstructures of Fe-Sb-C alloys of the medium-carbon series. Mag. 500X.

The microstructures of the high-carbon series of alloys are shown in Figure 25. The ε-phase does not appear until the 7.14 wt% Sb alloy of Figure 25c. In conjunction with the metallographic results of the binary alloy series, this would suggest that the solubility of ε is *not* significantly affected by the presence of carbon, a result contrary to that inferred from the metallography of the medium-carbon series. However, the absence of the ε-phase from the lower antimony alloys makes it difficult to explain some of the upcoming carbide extraction results. Therefore, the metallographic results are in themselves contradictory. The most reasonable interpretation appears to be that the solubility of antimony in the ferrite of all alloys, regardless of carbon content, is near 5 wt%.

The results of the electron probe microanalyses are presented in Table 5. The compositions reported for cementite and ε only indicate qualitative values relative to the matrix composition because of the previously mentioned problem of the unavoidable excitation of the adjacent matrix. One must conclude that there is considerable inhomogeneity in some of the structures (cf., the matrix compositions of Specimens D-6, D-10, and D-19-1). Nevertheless, the antimony concentration of the carbide phase in every case is reported to be less than that of the ferrite matrix, and the matrix composition in most cases is found to be richer in antimony than the overall composition (except where formation of the ε-phase would, of course, deplete the matrix of antimony). Thus a value of the distribution coefficient k of less than one is clearly indicated.

The analyses of the various carbide extracts are also presented in Table 5. Contrary to the electron probe analyses, these invariably resulted in an apparent antimony concentration in the carbide well in excess of the overall composition, indicating a distribution coefficient greater than one. This contradictory result could be explained if the extracts also contained some ε-phase along with the carbide. However, for some of the alloys the ε-phase should not have been present and, in fact, was not observed metallographically, nor was ε observed in the X-ray diffraction analysis. Thus for these specimens the result remains an anomaly.

The crystal structure was investigated and crystallographic lattice parameters determined from some of the extracted carbides. Data for the observed diffraction peaks obtained from carbides of the high-carbon series are presented in Table 6. The peaks were indexed assuming an orthorhombic structure and the lattice parameters calculated as described previously. These lattice parameters are plotted versus antimony concentration in Figure 27, showing little change in the volume of the unit cell with antimony content of the alloy. Assuming that antimony atoms will substitute for iron atoms on the cementite lattice to form a carbide of the type $(FeSb)_3C$, one would expect the unit cell dimensions to increase if the antimony atom is larger than iron. The fact that such an increase was not observed suggests that antimony is *not* partitioning to the carbide phase. However, this conclusion must be considered rather tenuous, based on this evidence, since it has been reported that the substitution of the larger chromium atom for iron on the cementite lattice can lead to a *reduction* in the size of the unit cell.[36] A few diffraction peaks from each of the specimens could conceivably be identified as part of the diffraction pattern of the ε-phase, suggesting the presence of ε in

36. WESTGREN, A., PHRAGMEN, G., and NEGRESCO, T. *On the Structure of the Iron-Chromium-Carbon System.* J. Iron Steel Inst., v. 117, 1928, p. 383-400.

a. Fe-1.54%Sb-0.57%C

b. Fe-2.57%Sb-0.53%C

c. Fe-7.14%Sb-0.46%C

d. Fe-14.28%Sb-0.46%C

Figure 25. Microstructures of Fe-Sb-C alloys of the high-carbon series. Mag. 500X.

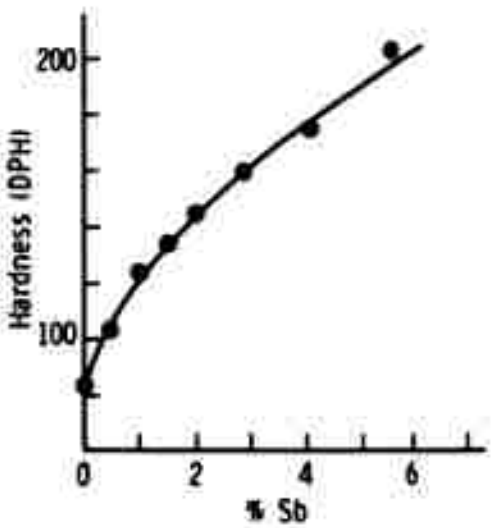

Figure 26. The hardening of ferrite by antimony.

Table 5. Fe-Sb AND Fe-Sb-C ALLOYS

Alloy No.	Composition %C	Composition %Sb	Electron Probe Analysis (% Sb) Ferrite Matrix	Intermetallic Carbide Phase (ε phase)	Intermetallic Overall	Carbide Extract %C	Carbide Extract %Sb	Ferrite Lattice Parameter†	
D-14	0.01	0.05						2.8669	
D-15	0.01	0.10						2.8670	
D-7	0.03	0.10	<0.07	-	-			2.8677	
D-4	0.02	0.47						2.8686	
D-9	0.03	0.47						2.8691	
D-1	0.02	0.48						2.8692	
D-16	0.01	0.49						2.8684	
D-2	0.03	0.97						2.8704	M=0.003443
D-5	0.01	0.98						2.8705	
D-17-1	0.01	1.44						2.8717	
D-6	0.01	1.94	1.96	-	-			2.8735	
D-18-1	0.02	2.84						2.8764	
D-19-1	0.01	4.07	2.60-5.37	-	5.60-5.97*	-		2.8807	
D-20-1	0.01	5.54						2.8856	
D-12-1	0.06	6.40	5.2	0.8	57.4	6.3		2.8852	
D-13-1	0.01	6.46	6.79-7.50	-	10.4-27.2*	6.61		2.8860	
D-23-1	0.02	15.10						2.8792	(400°C)
								2.8856	(600°C)
								2.8937	(800°C)
								2.8996	(950°C)
D-17	0.14	0.02						2.8668	
D-18	0.13	0.05						2.8674	
D-10	0.09	0.10	0.12	<0.07*	-	-	3.12-5.36 1.08-2.48	2.8675	M'=0.005040 k=-16.6
D-11	0.12	0.29					4.68-7.29 2.28-3.15	2.8681	
D-12	0.11	0.47						2.8689	
D-19	0.23	0.02					3.97-8.94 0.04-0.06	2.8672	M'=0.007157
D-13	0.24	0.45	0.59	0.08	-	-	1.72-6.70 3.25-5.24	2.8698	k=-14.0
D-20	0.29	0.05	0.59	0.08	-	-	5.23-9.58 0.14-0.22	2.8672	
D-16-1	0.36	1.45						2.8700	
D-14-1	0.35	2.80	3.9	0.8	59.0	2.2		2.8767	M'=0.003606 k=0.14
D-15-1	0.35	4.04	4.1	0.8	57.6	4.0		2.8811	
D-21-1	0.36	5.48	3.8	0.7	58.9	4.3		2.8864	
D-24-1	0.32	15.10						2.8863	
D-25-1	0.57	1.54						2.8716	
D-26-1	0.53	2.57					1.30 10.80	2.8763	M'=0.003603 k=0.44
D-27-1	0.53	4.38					6.80 18.90	2.8821	
D-28-1	0.46	7.14						2.8849	
D-29-1	0.46	14.28						2.8849	

†Annealed at 600 C unless otherwise indicated
*Includes excitation of adjacent areas

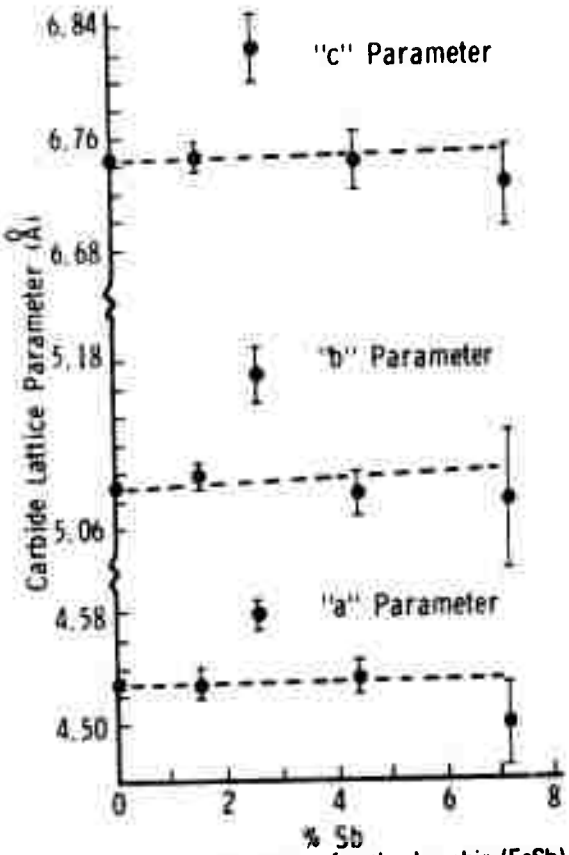

Figure 27. Lattice parameters of orthorhombic $(FeSb)_3C$ as a function of antimony concentration in Fe-Sb-C alloys of the high-carbon series.

the carbide extracts, but separation of the peaks to unequivocally show the presence of more than one phase was not possible. The anomalous result for the 2.57% Sb alloy suggests the presence of an antimony-rich carbide phase different from Fe_3C.

The ferrite lattice parameter data are contained in Table 5 and are also plotted versus antimony concentration in Figure 28. The expansion of the ferrite lattice is shown as expected in each case. Specimens of one binary alloy (D-23-1) were annealed for two weeks at 400, 600, 800, and 950 C and the lattice parameters measured, from which the limit of solubility of antimony in ferrite was determined. The resulting solvus line is shown in Figure 29. Previous measurements of the solid solubility of antimony in α-iron have produced varying results. The X-ray work of Hägg[29] gave the solubility as 6.3 wt% Sb at some unspecified low temperature. Geller[37] metallographically determined the solubility to be 8 wt% Sb at the eutectic temperature decreasing to 5 wt% Sb at room temperature. Fournier[38] reported a solubility of 12 wt% Sb at 950 C based on metallographic examination. The present results fall in this same range of solubilities, and are considered to give more accurate values than the previously cited results.

The solubility of the ε-phase at 600 C does not appear to be significantly affected by the presence of carbon; the medium- and high-carbon series alloys give roughly the same solid solubility. It may be recalled that medium-carbon series alloys with as little as 2.84 wt% Sb exhibited the presence of the ε-phase along with cementite and ferrite in the microstructure. If these alloys were showing true three-phase equilibrium, the ferrite composition would have remained fixed even though the antimony concentration in the alloys varied, and the ferrite lattice parameter would have been unchanged in all the alloys with antimony concentrations greater than that in which ε first appeared. Instead, the lattice parameter measurements show a continuous increase throughout this composition range, signifying a changing ferrite composition and hence no three-phase equilibrium. There does not appear to be any way of reconciling the X-ray and metallographic results short of assuming that the latter were affected by inhomogeneities in

37. GELLER, W. *The System Iron-Cobalt-Antimony.* Arch. Eisenhüttenw., v. 13, 1939, p. 263-266.
38. FOURNIER, P. *The Iron-Antimony System.* Rev. Chem. Ind., v. 44, 1935, p. 195-199.

Table 6. X-RAY DATA FROM CARBIDES EXTRACTED FROM Fe-Sb-C ALLOYS

hkl	Fe_3C (ASTM Standard)	Alloy C-6 0%Sb	D-25 1.54%Sb	D-26 2.57%Sb	D-27 4.38%Sb	D-28 7.14%Sb
020	2θ = I = VW* d = 2.54	53.167 VW 2.560	53.220 W 2.557	53.266 -M 2.555	53.667 S 2.538	53.333 VW 2.552
112/021	2θ = I = VS d = 2.38	56.967 VS 2.402	57.109 -S 2.397	57.266 -M 2.390	-	57.267 VW 2.390
200	2θ = I = M d = 2.26	60.433 M 2.276	60.561 W 2.272	60.667 -W 2.268	60.167 +W 2.285	-
120	2θ = I = M d = 2.23	-	-	62.067 -M 2.222	-	-
121	2θ = I = VS d = 2.10	65.444 VS 2.119	65.612 -S 2.114	65.755 M 2.110	66.167 W 2.099	66.433 -M 2.091
210	2θ = I = VS d = 2.06	66.866 VS 2.079	67.035 +M 2.075	67.170 -M 2.071	67.366 VW 2.066	67.633 M 2.058
103	2θ = I = VS d = 2.01	68.950 VS 2.024	69.121 VS 2.019	69.233 VS 2.016	69.566 VW 2.008	69.300 -M 2.015
211	2θ = I = VS d = 1.99	70.432 VS 1.986	70.595 -S 1.982	70.734 M 1.979	71.966 W 1.950	70.800 -W 1.978
113	2θ = I = -M d = 1.87	75.089 M 1.880	75.170 M 1.878	75.300 -M 1.875	-	75.367 VW 1.874
122	2θ = I = S - d = 1.86	-	-	76.233 -M 1.856	-	76.200 VW 1.857
212	2θ = I = -M d = 1.77	-	-	80.967 W 1.764	81.198 W 1.760	
004/023	2θ = I = -M d = 1.68	85.300 -M 1.691	85.447 -M 1.688	85.566 +W 1.687	-	85.733 +W 1.684
221	2θ = I = -W d = 1.61	88.260 -W 1.645	88.300 W 1.645	88.333 W 1.644	88.667 +W 1.639	-
130	2θ = I = -M d = 1.59			92.200 VW 1.590		
222	2θ = I = W d = 1.51			98.400 VW 1.513		
033	2θ = I = d =			112.000 VW 1.382		
320	2θ = I = d =			-		
322	2θ = I = d =			138.333 VW 1.226		

*Intensities: S = strong, M = medium, W = weak, V = very

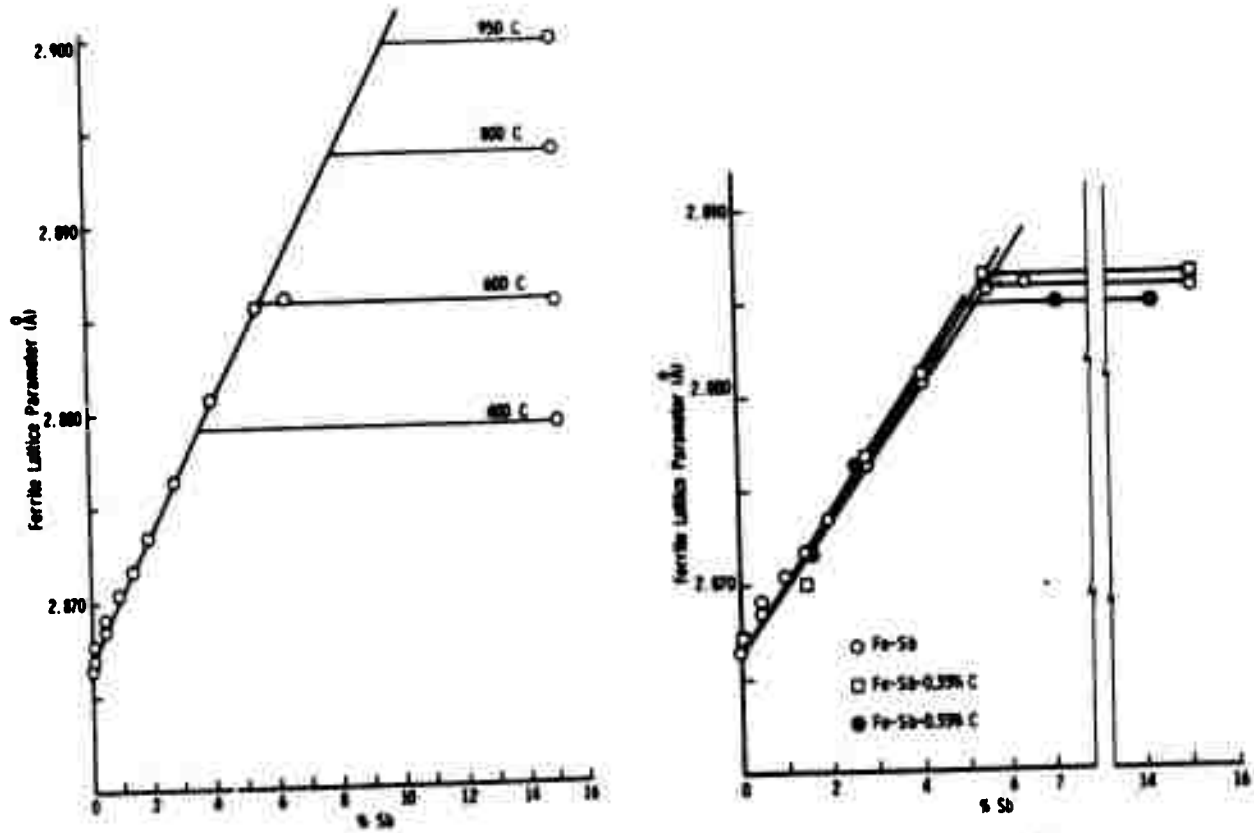

a. Fe-Sb binary alloys.

b. Fe-Sb and Fe-Sb-C alloys.

Figure 28. Ferrite lattice parameter as a function of antimony concentration. Alloys were annealed at 600 C unless otherwise indicated.

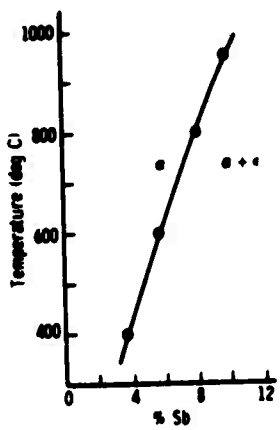

Figure 29. The iron-rich end of the iron-antimony binary phase diagram based upon present results, showing the α-solvus.

antimony composition. The X-ray results could have been affected by drastic decarburization of the specimens, causing them to appear as binary alloys, but it is felt that alloy inhomogeneity had the dominant effect.

The values of M' obtained from various groupings of alloys are presented in Table 5. In every case M' > M, signifying a distribution coefficient less than one. In fact, some values of k, as calculated from Equation (9), are negative (a physical impossibility). A negative k simply means that the calculated tie line in the "ferrite + carbide" two-phase region intercepts the edge of the phase diagram at a carbon content less than the carbon content of cementite. This is clearly in error, but it nevertheless confirms the fact that the equilibrium antimony concentration in the carbide is much less than the antimony concentration of the ferrite, and that k is less than one as is shown directly in the medium- and high-carbon series results.

Therefore, the X-ray and microprobe results both indicate a distribution coefficient of less than one, meaning that antimony will be rejected by the carbides and will dissolve substitutionally in the ferrite. Also the X-ray and metallographic results both suggest a solid solubility of antimony in ferrite of roughly 5 wt% Sb at 600 C, independent of carbon content. In spite of problems apparently caused by inhomogeneous alloys, the above two conclusions appear to be most consistently reflected in the experimental results.

Fe-As and Fe-As-C Alloys

The published binary Fe-As phase diagram[23] is shown in Figure 30. The alloy series containing arsenic may be divided into two groups (see Table 7): (1) a binary Fe-As series (%C∿0.01) and (2) a medium-carbon series (%C∿0.35). All alloys of this system were given homogenizing heat treatments at 800 C and then annealed for two weeks at 600 C. The microstructures of selected alloys from these two series are presented in Figures 31 and 32. The limit of solid solubility of arsenic in ferrite is not reached in either series of alloys until the arsenic concentration exceeds that of Specimen E-5 (Figure 31c) in the binary series consistent wih the published phase diagram, and Specimen E-10 (Figure 32b) of the medium-carbon series. The arsenic-rich phase formed beyond the solubility limit in the binary series is the intermetallic compound Fe_2As. It is not clear what phase is present with the ferrite in the highest arsenic alloy of the medium-carbon series (Figure 32c). Its volume fraction is too great for it to be a carbide; it may be a ternary Fe-As-C compound. The solid solution strengthening of ferrite by arsenic is illustrated by the hardness data of Figure 33.

The electron probe microanalysis results are presented in Table 7. It is consistently found that in the alloys containing carbides, the carbides show a depletion in arsenic. The corresponding enrichment of the ferrite that should accompany the carbide depletion is less consistently shown. Nevertheless the analyses most often point to a result which is characteristic of a distribution coefficient k less than one.

The ferrite lattice parameter measurements are presented in Table 7 and are also plotted versus the arsenic concentration in Figure 34. One binary series alloy containing 18.0 wt% As (Specimen E-13) was annealed at 400, 600, 700, and

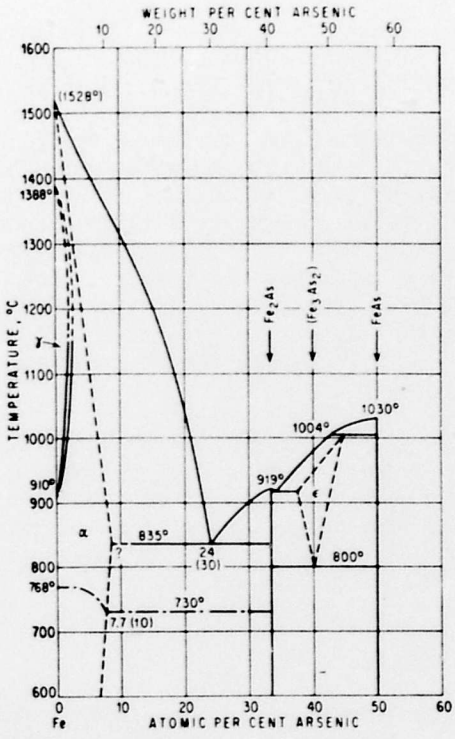

Figure 30. Iron-arsenic binary phase diagram (Reference 23). (Courtesy of McGraw-Hill Company)

Table 7. Fe-As AND Fe-As-C ALLOYS

Alloy No.	Composition %C	Composition %As	Electron Probe Analysis (% As) Ferrite Matrix	Carbide	Intermetallic Phase (Fe_2As)	Overall	Ferrite Lattice Parameter†	
E-1	0.01	1.28	. . . . .				2.8690	
E-2	0.01	2.64	. . . . .				2.8707	
E-3	0.01	3.98	. . . . .				2.8729	M=0.001623
E-4	0.01	4.78	3.98-4.35	-	-	4.16	2.8742	
E-5	0.01	5.37	3.15-5.05	-	-	5.00	2.8750	
E-13	0.01	18.00	. . . . .				2.8808	(400°C)
							2.8828	(600°C)
							2.8851	(700°C)
							2.8858	(800°C)
E-7	0.35	1.15	1.20-2.60	0.14-0.72*	-	1.00	2.8692	
E-8	0.35	2.73	2.26-4.50	0.20-1.22*	-	3.14	2.8715	M'=0.001809
E-9	0.36	3.39	3.14-4.92	1.03-1.62*	-	3.43	2.8728	k=-0.93
E-10	0.36	5.29	5.03-6.43	1.28-3.10	-	5.56	2.8760	
E-14	0.31	17.20	. . . . .				2.8836	

†Annealed at 600 C unless otherwise indicated
*Includes excitation of adjacent areas

a. Fe-2.64%As

b. Fe-3.98%As

c. Fe-5.37%As

d. Fe-18.00%As

Figure 31. Microstructures of alloys of the Fe-As binary series (%C∿0.01). Mag. 500X.

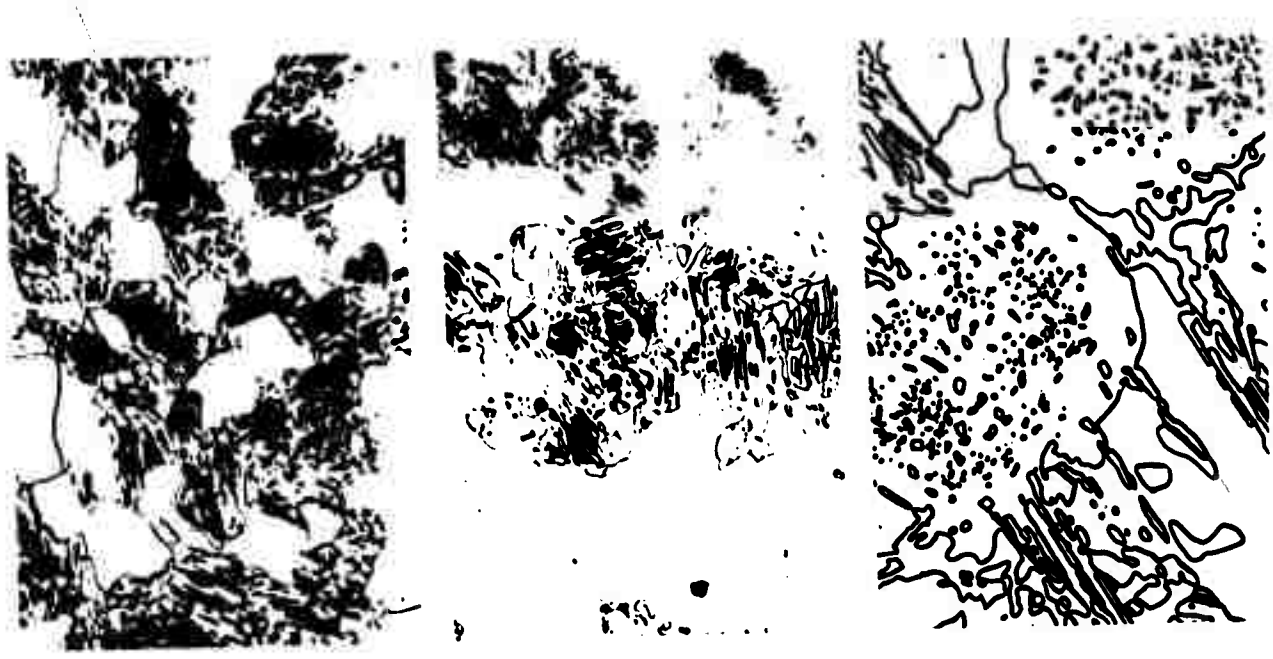

a. Fe-1.15%As-0.35%C

b. Fe-3.39%As-0.36%C

c. Fe-17.20%As-0.31%C

Figure 32. Microstructures of Fe-As-C alloys of the medium-carbon series. Mag. 500X.

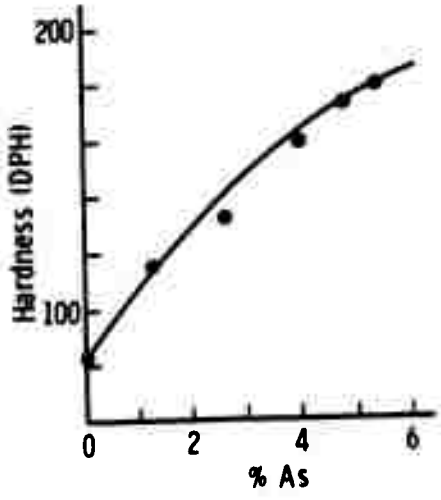

Figure 33. The hardening of ferrite by arsenic.

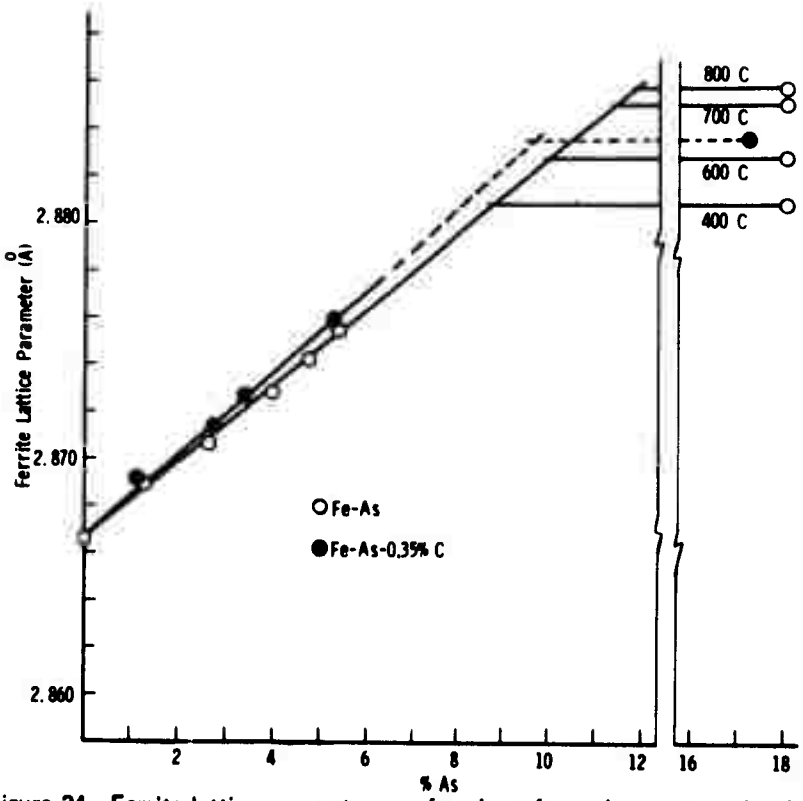

Figure 34. Ferrite lattice parameter as a function of arsenic concentration in Fe-As and Fe-As-C alloys, annealed at 600 C unless otherwise indicated.

800 C, and its resulting lattice parameters defined the limit of arsenic solubility at these temperatures. The solvus line determined from these data appears in Figure 35. This is in excellent agreement with other experimental determinations of arsenic solubility in ferrite.[39,40]

The solubility limit determined from the lattice parameter of the 17.2 wt% As medium-carbon alloy (see Figure 34) appears to indicate that carbon has little effect on the arsenic solubility in ferrite. However, the metallographic results did not show this alloy to consist of the three phases ferrite, cementite, and Fe_2As, so that the solubility limit given may not necessarily represent the position of the ferrite corner of that particular three-phase region of the ternary phase diagram.

The values of M and M' determined from Figure 34 show M' > M, signifying a distribution coefficient k less than one. Calculating k from Equation (9) gives the result k = -0.93. Once again the negative value of k corresponds to a computed tie line in the "ferrite + carbide" two-phase region which intercepts the edge of the ternary phase diagram at a carbon content less than the carbon content of cementite. This physical impossibility nonetheless gives strong support for the

39. SVECHNIKOV, V. N., PAN, V. M., and SHURIN, A. K. *Effect of Phosphorus and Arsenic on the Crystal Lattice Parameter and the Hardness of Alpha-Iron.* Phys. Metals Metallog., v. 6, 1958, p. 80-82.
40. SVECHNIKOV, V. N., and SHURIN, A. K. *A More Precise Determination of the Equilibrium Diagram of an Fe-As System.* Dopovidi Akad, Nauk Ukr. RSR, 1957(1), p. 27-29.

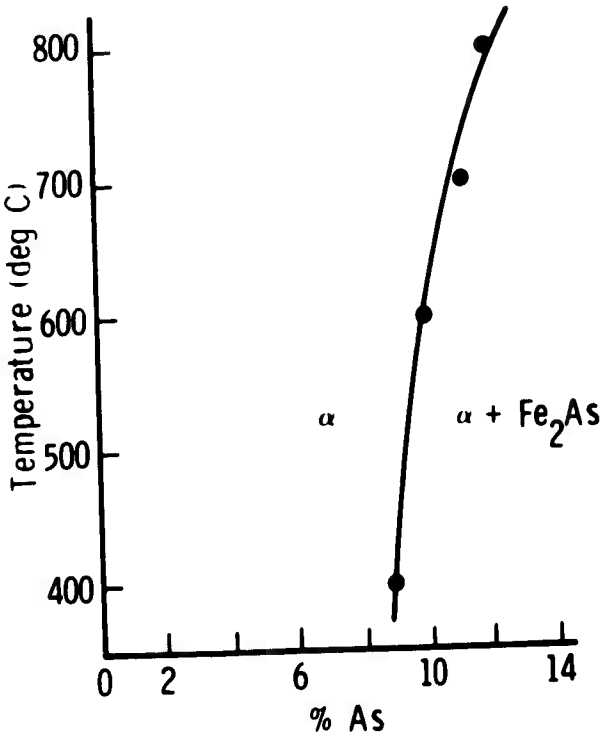

Figure 35. Iron-rich end of the iron-arsenic binary phase diagram based upon present results, showing the α-solvus.

argument that the solubility of arsenic in cementite is very small, and that k is much less than one. This is consistent with the electron microprobe results and is also consistent with the Fe-As-C phase diagram determination at higher temperatures by Sawamura and Mori.[41] Thus arsenic would tend to be rejected by the carbide and would accumulate on the ferrite side of the ferrite/carbide interface.

SUMMARY AND CONCLUSIONS

The occurrence of intergranular embrittlement in steels implies that the character of the ferrite matrix in the vicinity of the grain boundary or ferrite/carbide interface, or the character of the interface itself, has been altered in some way such that the normal deformation processes that occur in a ductile steel are now impeded. One might postulate that the partitioning of impurity elements between the ferrite matrix and the carbides formed on tempering lead to such an alteration by causing impurities to accumulate on one side of the interface or the other during the partitioning process. Inasmuch as ferrite is the ductile phase, one might anticipate that impurities which accumulate on the ferrite side of the interface would have the greater effect. Furthermore, impurities which produce the most solid-solution hardening of the ferrite are presumably most effective in impeding dislocation motion and hence deformation, and so these impurities might be expected to be the most damaging embrittling agents.

41. SAWAMURA, H., and MORI, T. *An Investigation of Equilibrium Diagram of Fe-As-C System.* Mem. Fac. Eng. Kyoto Univ., v. 14, 1952, p. 129-144.

This study has shown the elements tin, phosphorus, silicon, antimony, and arsenic all to be potent ferrite strengtheners (cf. Figures 7, 15, 20, 26, and 33). As the solubility limit in ferrite is approached, the diamond pyramid hardnesses due to Si, Sn, Sb, As and P are approximately 450, 300, 200, 200, and 180, respectively, as compared to a hardness of about 80 for unalloyed ferrite. (On a unit concentration basis, i.e., the hardness increase produced by 1% of the impurity, these elements would rank in the order: P, Sb, Si, Sn, and As.) Of these elements, only tin and phosphorus appear to partition to the carbide phase, tin doing so quite strongly. The remaining elements silicon, antimony, and arsenic partition to ferrite and so would tend to accumulate on the ferrite side of the ferrite/carbide interface. Therefore, based on the above rationale, one might anticipate the most damaging effects from antimony and silicon, with the least effect caused by arsenic. The work of Low et al.[9] did in fact show antimony to have the greatest effect in causing temper embrittlement and arsenic the least, but they also show a strong effect due to tin. The strong embrittling effect due to tin, however, may be associated in some way with the tendency to form a ternary carbide in this system, which was the only system shown by the present investigation to exhibit this tendency. Coupled with these effects is the probability that the character of the ferrite/carbide interface itself plays a role in the embrittlement process.

TECHNICAL REPORT DISTRIBUTION

No. of Copies	To
1	Office of the Director, Defense Research and Engineering, The Pentagon, Washington, D. C. 20301
12	Commander, Defense Documentation Center, Cameron Station, Building 5, 5010 Duke Street, Alexandria, Virginia 22314
1	Metals and Ceramics Information Center, Battelle Memorial Institute, 505 King Avenue, Columbus, Ohio 43201
1	Chemical Propulsion Information Agency, Applied Physics Laboratory, The Johns Hopkins University, 8621 Georgia Avenue, Silver Spring, Maryland 20910
	Chief of Research and Development, Department of the Army, Washington, D. C. 20310
2	ATTN: Physical and Engineering Sciences Division
	Commander, Army Research Office, P. O. Box 12211, Research Triangle Park, North Carolina 27709
1	ATTN: Information Processing Office
	Commander, U. S. Army Materiel Command, 5001 Eisenhower Avenue, Alexandria, Virginia 22333
1	ATTN: AMCRD-TC
1	AMCSA-S, Dr. R. B. Dillaway, Chief Scientist
	Commander, U. S. Army Electronics Command, Fort Monmouth, New Jersey 07703
1	ATTN: AMSEL-GG-DD
1	AMSEL-GG-DM
	Commander, U. S. Army Missile Command, Redstone Arsenal, Alabama 35809
1	ATTN: Technical Library
1	AMSMI-RSM, Mr. E. J. Wheelahan
	Commander, U. S. Army Armament Command, Rock Island, Illinois 61201
2	ATTN: Technical Library
	Commander, U. S. Army Natick Laboratories, Natick, Massachusetts 01760
1	ATTN: Technical Library
	Commander, U. S. Army Satellite Communications Agency, Fort Monmouth, New Jersey 07703
1	ATTN: Technical Document Center
	Commander, U. S. Army Tank-Automotive Command, Warren, Michigan 48090
2	ATTN: AMSTA-BSL, Research Library Branch

No. of Copies	To
	Commander, White Sands Missile Range, New Mexico 88002
1	ATTN: STEWS-WS-VT
	Commander, Aberdeen Proving Ground, Maryland 21005
1	ATTN: STEAP-TL, Bldg. 305
	President, Airborne, Electronics and Special Warfare Board, Fort Bragg, North Carolina 28307
1	ATTN: Library
	Commander, Dugway Proving Ground, Dugway, Utah 84022
1	ATTN: Technical Library, Technical Information Division
	Commander, Edgewood Arsenal, Maryland 21010
1	ATTN: Mr. F. E. Thompson, Dir. of Eng. & Ind. Serv., Chem-Mun Br
	Commander, Frankford Arsenal, Philadelphia, Pennsylvania 19137
1	ATTN: Library, H1300, Bl. 51-2
1	SMUFA-L300, Mr. J. Corrie
	Commander, Harry Diamond Laboratories, 2800 Powder Mill Road, Adelphi, Maryland 20783
1	ATTN: Technical Information Office
	Commander, Picatinny Arsenal, Dover, New Jersey 07801
1	ATTN: SMUPA-RT-S
	Commander, Redstone Scientific Information Center, U. S. Army Missile Command, Redstone Arsenal, Alabama 35809
4	ATTN: AMSMI-RBLD, Document Section
	Commander, Watervliet Arsenal, Watervliet, New York 12189
1	ATTN: SWEWV-RDT, Technical Information Services Office
	Commander, U. S. Army Foreign Science and Technology Center, 220 7th Street, N. E., Charlottesville, Virginia 22901
1	ATTN: AMXST-SD3
	Director, Eustis Directorate, U. S. Army Air Mobility Research and Development Laboratory, Fort Eustis, Virginia 23604
1	ATTN: Mr. J. Robinson, SAVDL-EU-SS
	Librarian, U. S. Army Aviation School Library, Fort Rucker, Alabama 36360
1	ATTN: Building 5907
	Commander, U. S. Army Engineer School, Fort Belvoir, Virginia 22060
1	ATTN: Library

No. of Copies	To
	Commandant, U. S. Army Quartermaster School, Fort Lee, Virginia 23801
1	ATTN: Quartermaster School Library
	Naval Research Laboratory, Washington, D. C. 20375
1	ATTN: Dr. J. M. Krafft - Code 8430
2	Dr. G. R. Yoder - Code 6382
	Chief of Naval Research, Arlington, Virginia 22217
1	ATTN: Code 471
	Air Force Materials Laboratory, Wright-Patterson Air Force Base, Ohio 45433
2	ATTN: AFML (MXE), E. Morrissey
1	AFML (LC)
1	AFML (LMD), D. M. Forney
	National Aeronautics and Space Administration, Washington, D. C. 20546
1	ATTN: Mr. B. G. Achhammer
1	Mr. G. C. Deutsch - Code RR-1
	National Aeronautics and Space Administration, Marshall Space Flight Center, Huntsville, Alabama 35812
1	ATTN: R-P&VE-M, R. J. Schwinghamer
1	S&E-ME-MM, Mr. W. A. Wilson, Building 4720
1	Ship Research Committee, Maritime Transportation Research Board, National Research Council, 2101 Constitution Ave., N. W., Washington, D. C. 20418
	P. R. Mallory Company, Inc., 3029 East Washington Street, Indianapolis, Indiana 46206
1	ATTN: Technical Library
1	Materials Sciences Corporation, Blue Bell Campus, Merion Towle Building, Blue Bell, Pennsylvania 19422
1	The Charles Stark Draper Laboratory, 68 Albany Street, Cambridge, Massachusetts 02139
	Wyman-Gordon Company, Worcester, Massachusetts 01601
1	ATTN: Technical Library
	Director, Army Materials and Mechanics Research Center, Watertown, Massachusetts 02172
2	ATTN: AMXMR-PL
1	AMXMR-AG
1	AMXMR-CT
1	AMXMR-XC
1	AMXMR-E
3	Authors
75	TOTAL COPIES DISTRIBUTED

Army Materials and Mechanics Research Center,
Watertown, Massachusetts 02172
THE PARTITIONING OF IMPURITY ELEMENTS
IN IRON-CARBON ALLOYS -
Weily F. Chiao, Gordon A. Bruggeman,
and Eric B. Kula

Technical Report AMMRC TR 75-19, September 1975, 42 pp -
illus-tables, D/A Project 1T16205AH84,
AMCMS Code 62105.11.H8400

AD________________
UNCLASSIFIED
UNLIMITED DISTRIBUTION

Key Words

Equilibrium
Chemical composition
Carbides

The partitioning at 600 C of tin, phosphorus, silicon, antimony, and arsenic between the ferrite and carbide phases was investigated in Fe-C-X alloys, where X is one of the above elements. These elements are all known to increase the susceptibility for temper brittleness in steels and are suspected of playing a similar role in the phenomenon of tempered martensite embrittlement or 500 F embrittlement. The procedures of metallographic examination, electron microprobe analysis, ferrite lattice parameter measurement, and chemical analysis and crystal structure determination of extracted carbides were employed. It was determined that only Sn and P appear to partition to the carbide phase, Sn apparently forming a ternary carbide. The remaining elements Si, Sb, and As partition to ferrite, thus providing a condition conducive to the accumulation of these impurities on the ferrite side of ferrite/carbide interfaces during tempering. By virtue of its more potent solid solution strengthening effect in ferrite, a greater embrittling tendency from Sb may be anticipated, a prediction borne out by experiment. Solubility limits, distribution coefficients, and other phase relations were determined.

Army Materials and Mechanics Research Center,
Watertown, Massachusetts 02172
THE PARTITIONING OF IMPURITY ELEMENTS
IN IRON-CARBON ALLOYS -
Weily F. Chiao, Gordon A. Bruggeman,
and Eric B. Kula

Technical Report AMMRC TR 75-19, September 1975, 42 pp -
illus-tables, D/A Project 1T16205AH84,
AMCMS Code 62105.11.H8400

AD________________
UNCLASSIFIED
UNLIMITED DISTRIBUTION

Key Words

Equilibrium
Chemical composition
Carbides

The partitioning at 600 C of tin, phosphorus, silicon, antimony, and arsenic between the ferrite and carbide phases was investigated in Fe-C-X alloys, where X is one of the above elements. These elements are all known to increase the susceptibility for temper brittleness in steels and are suspected of playing a similar role in the phenomenon of tempered martensite embrittlement or 500 F embrittlement. The procedures of metallographic examination, electron microprobe analysis, ferrite lattice parameter measurement, and chemical analysis and crystal structure determination of extracted carbides were employed. It was determined that only Sn and P appear to partition to the carbide phase, Sn apparently forming a ternary carbide. The remaining elements Si, Sb, and As partition to ferrite, thus providing a condition conducive to the accumulation of these impurities on the ferrite side of ferrite/carbide interfaces during tempering. By virtue of its more potent solid solution strengthening effect in ferrite, a greater embrittling tendency from Sb may be anticipated, a prediction borne out by experiment. Solubility limits, distribution coefficients, and other phase relations were determined.

Army Materials and Mechanics Research Center,
Watertown, Massachusetts 02172
THE PARTITIONING OF IMPURITY ELEMENTS
IN IRON-CARBON ALLOYS -
Weily F. Chiao, Gordon A. Bruggeman,
and Eric B. Kula

Technical Report AMMRC TR 75-19, September 1975, 42 pp -
illus-tables, D/A Project 1T16205AH84,
AMCMS Code 62105.11.H8400

AD________________
UNCLASSIFIED
UNLIMITED DISTRIBUTION

Key Words

Equilibrium
Chemical composition
Carbides

The partitioning at 600 C of tin, phosphorus, silicon, antimony, and arsenic between the ferrite and carbide phases was investigated in Fe-C-X alloys, where X is one of the above elements. These elements are all known to increase the susceptibility for temper brittleness in steels and are suspected of playing a similar role in the phenomenon of tempered martensite embrittlement or 500 F embrittlement. The procedures of metallographic examination, electron microprobe analysis, ferrite lattice parameter measurement, and chemical analysis and crystal structure determination of extracted carbides were employed. It was determined that only Sn and P appear to partition to the carbide phase, Sn apparently forming a ternary carbide. The remaining elements Si, Sb, and As partition to ferrite, thus providing a condition conducive to the accumulation of these impurities on the ferrite side of ferrite/carbide interfaces during tempering. By virtue of its more potent solid solution strengthening effect in ferrite, a greater embrittling tendency from Sb may be anticipated, a prediction borne out by experiment. Solubility limits, distribution coefficients, and other phase relations were determined.

Army Materials and Mechanics Research Center,
Watertown, Massachusetts 02172
THE PARTITIONING OF IMPURITY ELEMENTS
IN IRON-CARBON ALLOYS -
Weily F. Chiao, Gordon A. Bruggeman,
and Eric B. Kula

Technical Report AMMRC TR 75-19, September 1975, 42 pp -
illus-tables, D/A Project 1T16205AH84,
AMCMS Code 62105.11.H8400

AD________________
UNCLASSIFIED
UNLIMITED DISTRIBUTION

Key Words

Equilibrium
Chemical composition
Carbides

The partitioning at 600 C of tin, phosphorus, silicon, antimony, and arsenic between the ferrite and carbide phases was investigated in Fe-C-X alloys, where X is one of the above elements. These elements are all known to increase the susceptibility for temper brittleness in steels and are suspected of playing a similar role in the phenomenon of tempered martensite embrittlement or 500 F embrittlement. The procedures of metallographic examination, electron microprobe analysis, ferrite lattice parameter measurement, and chemical analysis and crystal structure determination of extracted carbides were employed. It was determined that only Sn and P appear to partition to the carbide phase, Sn apparently forming a ternary carbide. The remaining elements Si, Sb, and As partition to ferrite, thus providing a condition conducive to the accumulation of these impurities on the ferrite side of ferrite/carbide interfaces during tempering. By virtue of its more potent solid solution strengthening effect in ferrite, a greater embrittling tendency from Sb may be anticipated, a prediction borne out by experiment. Solubility limits, distribution coefficients, and other phase relations were determined.

Army Materials and Mechanics Research Center,
Watertown, Massachusetts 02172
THE PARTITIONING OF IMPURITY ELEMENTS
IN IRON-CARBON ALLOYS -
Weily F. Chiao, Gordon A. Bruggeman,
and Eric B. Kula

Technical Report AMMRC TR 75-19, September 1975, 42 pp -
illus-tables, D/A Project 1T16205AH84,
AMCMS Code 62105.11.H8400

AD________________
UNCLASSIFIED
UNLIMITED DISTRIBUTION

Key Words

Equilibrium
Chemical composition
Carbides

The partitioning at 600 C of tin, phosphorus, silicon, antimony, and arsenic between the ferrite and carbide phases was investigated in Fe-C-X alloys, where X is one of the above elements. These elements are all known to increase the susceptibility for temper brittleness in steels and are suspected of playing a similar role in the phenomenon of tempered martensite embrittlement or 500 F embrittlement. The procedures of metallographic examination, electron microprobe analysis, ferrite lattice parameter measurement, and chemical analysis and crystal structure determination of extracted carbides were employed. It was determined that only Sn and P appear to partition to the carbide phase, Sn apparently forming a ternary carbide. The remaining elements Si, Sb, and As partition to ferrite, thus providing a condition conducive to the accumulation of these impurities on the ferrite side of ferrite/carbide interfaces during tempering. By virtue of its more potent solid solution strengthening effect in ferrite, a greater embrittling tendency from Sb may be anticipated, a prediction borne out by experiment. Solubility limits, distribution coefficients, and other phase relations were determined.

Army Materials and Mechanics Research Center,
Watertown, Massachusetts 02172
THE PARTITIONING OF IMPURITY ELEMENTS
IN IRON-CARBON ALLOYS -
Weily F. Chiao, Gordon A. Bruggeman,
and Eric B. Kula

Technical Report AMMRC TR 75-19, September 1975, 42 pp -
illus-tables, D/A Project 1T16205AH84,
AMCMS Code 62105.11.H8400

AD________________
UNCLASSIFIED
UNLIMITED DISTRIBUTION

Key Words

Equilibrium
Chemical composition
Carbides

The partitioning at 600 C of tin, phosphorus, silicon, antimony, and arsenic between the ferrite and carbide phases was investigated in Fe-C-X alloys, where X is one of the above elements. These elements are all known to increase the susceptibility for temper brittleness in steels and are suspected of playing a similar role in the phenomenon of tempered martensite embrittlement or 500 F embrittlement. The procedures of metallographic examination, electron microprobe analysis, ferrite lattice parameter measurement, and chemical analysis and crystal structure determination of extracted carbides were employed. It was determined that only Sn and P appear to partition to the carbide phase, Sn apparently forming a ternary carbide. The remaining elements Si, Sb, and As partition to ferrite, thus providing a condition conducive to the accumulation of these impurities on the ferrite side of ferrite/carbide interfaces during tempering. By virtue of its more potent solid solution strengthening effect in ferrite, a greater embrittling tendency from Sb may be anticipated, a prediction borne out by experiment. Solubility limits, distribution coefficients, and other phase relations were determined.

Army Materials and Mechanics Research Center,
Watertown, Massachusetts 02172
THE PARTITIONING OF IMPURITY ELEMENTS
IN IRON-CARBON ALLOYS -
Weily F. Chiao, Gordon A. Bruggeman,
and Eric B. Kula

Technical Report AMMRC TR 75-19, September 1975, 42 pp -
illus-tables, D/A Project 1T16205AH84,
AMCMS Code 62105.11.H8400

AD________________
UNCLASSIFIED
UNLIMITED DISTRIBUTION

Key Words

Equilibrium
Chemical composition
Carbides

The partitioning at 600 C of tin, phosphorus, silicon, antimony, and arsenic between the ferrite and carbide phases was investigated in Fe-C-X alloys, where X is one of the above elements. These elements are all known to increase the susceptibility for temper brittleness in steels and are suspected of playing a similar role in the phenomenon of tempered martensite embrittlement or 500 F embrittlement. The procedures of metallographic examination, electron microprobe analysis, ferrite lattice parameter measurement, and chemical analysis and crystal structure determination of extracted carbides were employed. It was determined that only Sn and P appear to partition to the carbide phase, Sn apparently forming a ternary carbide. The remaining elements Si, Sb, and As partition to ferrite, thus providing a condition conducive to the accumulation of these impurities on the ferrite side of ferrite/carbide interfaces during tempering. By virtue of its more potent solid solution strengthening effect in ferrite, a greater embrittling tendency from Sb may be anticipated, a prediction borne out by experiment. Solubility limits, distribution coefficients, and other phase relations were determined.

Army Materials and Mechanics Research Center,
Watertown, Massachusetts 02172
THE PARTITIONING OF IMPURITY ELEMENTS
IN IRON-CARBON ALLOYS -
Weily F. Chiao, Gordon A. Bruggeman,
and Eric B. Kula

Technical Report AMMRC TR 75-19, September 1975, 42 pp -
illus-tables, D/A Project 1T16205AH84,
AMCMS Code 62105.11.H8400

AD________________
UNCLASSIFIED
UNLIMITED DISTRIBUTION

Key Words

Equilibrium
Chemical composition
Carbides

The partitioning at 600 C of tin, phosphorus, silicon, antimony, and arsenic between the ferrite and carbide phases was investigated in Fe-C-X alloys, where X is one of the above elements. These elements are all known to increase the susceptibility for temper brittleness in steels and are suspected of playing a similar role in the phenomenon of tempered martensite embrittlement or 500 F embrittlement. The procedures of metallographic examination, electron microprobe analysis, ferrite lattice parameter measurement, and chemical analysis and crystal structure determination of extracted carbides were employed. It was determined that only Sn and P appear to partition to the carbide phase, Sn apparently forming a ternary carbide. The remaining elements Si, Sb, and As partition to ferrite, thus providing a condition conducive to the accumulation of these impurities on the ferrite side of ferrite/carbide interfaces during tempering. By virtue of its more potent solid solution strengthening effect in ferrite, a greater embrittling tendency from Sb may be anticipated, a prediction borne out by experiment. Solubility limits, distribution coefficients, and other phase relations were determined.